JCB Journal of Cell Biology

ARTICLE

Clathrin adaptors mediate two sequential pathways of intra-Golgi recycling

Jason C. Casler, Natalie Johnson, Adam H. Krahn, Areti Pantazopoulou, Kasey J. Day, and Benjamin S. Glick

The pathways of membrane traffic within the Golgi apparatus are not fully known. This question was addressed using the yeast *Saccharomyces cerevisiae*, in which the maturation of individual Golgi cisternae can be visualized. We recently proposed that the AP-1 clathrin adaptor mediates intra-Golgi recycling late in the process of cisternal maturation. Here, we demonstrate that AP-1 cooperates with the Ent5 clathrin adaptor to recycle a set of Golgi transmembrane proteins, including some that were previously thought to pass through endosomes. This recycling can be detected by removing AP-1 and Ent5, thereby diverting the AP-1/Ent5–dependent Golgi proteins into an alternative recycling loop that involves traffic to the plasma membrane followed by endocytosis. Unexpectedly, various AP-1/Ent5–dependent Golgi proteins show either intermediate or late kinetics of residence in maturing cisternae. We infer that the AP-1/Ent5 pair mediates two sequential intra-Golgi recycling pathways that define two classes of Golgi proteins. This insight can explain the polarized distribution of transmembrane proteins in the Golgi.

Introduction

The structure and composition of the Golgi apparatus are well described. In many cell types, including animal and plant cells, the Golgi consists of stacks of disk-like cisternae (Farquhar and Palade, 1981). In other organisms such as the budding yeast *Saccharomyces cerevisiae*, the cisternae are not stacked (Mowbrey and Dacks, 2009; Papanikou and Glick, 2009). Despite these differences in organization, the basic functions of the Golgi are conserved. Newly synthesized cargo proteins arrive at the Golgi from the ER, advance from early to late cisternae, and ultimately depart from the TGN to either the plasma membrane or the endosomal/lysosomal/vacuolar system (De Matteis and Luini, 2008). Golgi resident transmembrane proteins include components involved in membrane traffic as well as enzymes involved in the glycosylation and proteolytic processing of cargo molecules (Banfield, 2011). On the surface of Golgi cisternae are peripheral membrane proteins that include GTPases, vesicle coat proteins, and vesicle tethers. These peripheral membrane proteins cooperate with lipids and transmembrane proteins to drive traffic to, from, and within the Golgi (Munro, 2002; Gillingham and Munro, 2016; Thomas and Fromme, 2020). The components of the Golgi are being extensively characterized in biochemical and structural terms.

Less is known about the broader operating principles of the Golgi machine. Increasing evidence favors a cisternal maturation model in which Golgi cisternae assemble de novo from ER-derived membranes, progressively mature, and ultimately disintegrate at the TGN stage by forming secretory vesicles and other carriers (Glick and Luini, 2011). Golgi maturation can be visualized directly in *S. cerevisiae* by labeling resident Golgi proteins with fluorescent tags and then observing the arrival and departure of the tagged proteins in individual cisternae (Glick and Nakano, 2009). Although the dynamic properties of the Golgi are still debated for mammalian cells (Patterson et al., 2008; Pfeffer, 2010; Pellett et al., 2013), diverse experimental findings combined with the strong conservation of membrane traffic components support the generality of cisternal maturation (Glick and Nakano, 2009).

The maturation model could offer a solution to the long-standing mystery of Golgi polarity (Glick et al., 1997; Tu and Banfield, 2010; Welch and Munro, 2019). In a stacked Golgi, some resident transmembrane proteins are concentrated at the cis side of the stack, whereas others are concentrated in the middle of the stack or at the trans side (Dunphy and Rothman, 1985; Rabouille et al., 1995; Tie et al., 2016). A similar polarized distribution is seen in the nonstacked Golgi of *S. cerevisiae* (Kim et al., 2016; Day et al., 2018; Tojima et al., 2019). These observations led to the view that the Golgi consists of compartments designated cis, medial/trans, and TGN (Dunphy and Rothman, 1985; Mellman and Simons, 1992). Yet according to the maturation model, each cis cisterna matures into a medial/

Department of Molecular Genetics and Cell Biology, The University of Chicago, Chicago, IL.

Correspondence to Benjamin S. Glick: bsglick@uchicago.edu.

trans cisterna and then into a TGN cisterna, while resident Golgi proteins recycle from older to younger cisternae. We have proposed that the Golgi should be seen not as a set of compartments, but rather as a set of maturing cisternae controlled by a molecular logic circuit that switches membrane traffic pathways on and off in a particular sequence (Pantazopoulou and Glick, 2019). The recycling pathway of a transmembrane Golgi protein would determine when that protein resides in a maturing cisterna. Thus, each recycling pathway would define a class of transmembrane Golgi proteins, and these different classes of proteins would show distinct kinetic signatures and distinct patterns of concentration in the cisternae.

To test this idea, we need to determine which membrane recycling pathways operate at the Golgi and when. COPI-coated vesicles have been shown to mediate Golgi-to-ER recycling and intra-Golgi recycling of certain transmembrane proteins (Rabouille and Klumperman, 2005; Barlowe and Miller, 2013). In yeast, COPI is present during approximately the first half of the maturation process and seems to act selectively in the recycling of early Golgi proteins (Papanikou et al., 2015; Ishii et al., 2016; Kim et al., 2016). Our data suggested that recycling of some late Golgi proteins might involve clathrin-coated vesicles that form with the aid of the AP-1 adaptor (Papanikou et al., 2015; Day et al., 2018; Casler and Glick, 2019). Yeast AP-1 has been implicated in the recycling of transmembrane TGN proteins (Valdivia et al., 2002; Foote and Nothwehr, 2006; Liu et al., 2008; Spang, 2015), and we found that AP-1 is restricted to the TGN, implying that AP-1 mediates intra-Golgi recycling downstream of COPI (Day et al., 2018).

Yeast AP-1 interacts with the epsin-related clathrin adaptor Ent5 (Duncan et al., 2003; Costaguta et al., 2006; Čopič et al., 2007). These two adaptors have partially overlapping functions and can act independently. It therefore seems likely that AP-1 and Ent5 cooperate at the TGN to recycle Golgi transmembrane proteins. However, little is known about which Golgi proteins might be AP-1/Ent5 dependent.

This question could be addressed by deleting AP-1 and Ent5 simultaneously, but yeast strains lacking both AP-1 and Ent5 show only mild phenotypes (Costaguta et al., 2006). A possible explanation is that in the absence of AP-1 and Ent5, some Golgi proteins reach the plasma membrane and then recycle by endocytosis (Valdivia et al., 2002; Liu et al., 2008). Such a bypass mechanism for AP-1/Ent5–dependent proteins is easy to picture because the yeast Golgi also serves as an early endosome, with endocytic vesicles fusing around the time that an early Golgi cisterna matures into a TGN cisterna (Day et al., 2018). We now demonstrate that simultaneous removal of AP-1 and Ent5 does indeed cause a set of Golgi transmembrane proteins to recycle via the plasma membrane. The prevalence of AP-1/Ent5–dependent recycling was not appreciated because TGN proteins were thought to localize by retrieval from prevacuolar endosome (PVE) compartments (Conibear and Stevens, 1998), whereas our data indicate that many TGN proteins actually undergo intra-Golgi recycling.

Surprisingly, AP-1/Ent5–dependent Golgi proteins fall into two kinetic classes. As stated above, AP-1/Ent5 plays a role in recycling proteins that reside in the Golgi during a late phase of maturation and that have been designated TGN residents. AP-1/Ent5 also plays a role in recycling proteins that reside in the Golgi during an intermediate phase of maturation and that have been designated medial/trans residents. The AP-1/Ent5 pair apparently mediates two sequential pathways of intra-Golgi recycling.

We find that the recycling pathways at the Golgi show varying degrees of temporal overlap. A given cisterna may contain transmembrane proteins that follow several pathways, so classifying individual cisternae according to their resident protein compositions has limited value. Instead, classifying individual Golgi transmembrane proteins according to their recycling pathways offers a precise way to characterize the polarized composition of the Golgi.

Results

The AP-1/Ent5 pair recycles membrane during TGN maturation

Payne and colleagues reported that AP-1 and Ent5 showed similar kinetic signatures late in the process of yeast TGN maturation, although the data hinted at some differences between the two adaptors (Daboussi et al., 2012). To obtain a clear view of AP-1 and Ent5 kinetics, we devised a procedure for smoothing and averaging the noisy fluorescence traces obtained from analyzing individual cisternae by 4D confocal microscopy. Fig. 1 A shows frames from Video 1, in which a yeast strain expressed the TGN marker Sec7-mScarlet together with the AP-1 subunit Apl2-GFP plus Ent5-HaloTag coupled to the far-red dye JFX_{646} (Losev et al., 2006; Casler et al., 2019; Grimm et al., 2021). A representative cisterna was chosen for analysis. In accord with prior results (Day et al., 2018; Casler et al., 2019), AP-1 arrived about halfway through the Sec7 time course and departed shortly after Sec7. Fig. 1 B shows quantification of the fluorescence signals from this cisterna. In Fig. 1 C, the traces from 18 such events were smoothed and averaged. The results indicate that for a typical cisterna, Ent5 arrives a few seconds before AP-1, accumulates to its maximal level faster than AP-1, and begins to depart while AP-1 levels are still rising. Thus, AP-1 and Ent5 overlap substantially during TGN maturation but show distinct kinetic signatures. The AP-1/Ent5 pair is a candidate for mediating membrane recycling from maturing TGN cisternae.

To test this hypothesis, we revisited an apparent paradox: when the bulk membrane marker dye FM 4–64 was internalized by endocytosis to the yeast TGN, dye signal persisted in the TGN for many minutes even though TGN cisternae turn over on a much faster time scale (Day et al., 2018). Our proposed explanation was that membrane components continually recycle from older to younger TGN cisternae (Day et al., 2018). We therefore predicted that removal of AP-1/Ent5 would reduce the persistence of FM 4–64 in the TGN. Fig. 1 D shows internalized FM 4–64 after a 3-min pulse followed by a 5- or 10-min chase in cells expressing Sec7-GFP. In a wild-type strain, FM 4–64 was visible in many of the Sec7-containing cisternae at both time points. By contrast, in a strain lacking both Ent5 and the AP-1 subunit Apl4, FM 4–64 was readily detected in Sec7-containing cisternae only at the 5-min time point. At the 10-min time point in the *apl4Δ ent5Δ* strain, FM 4–64 was often seen at sites of polarized

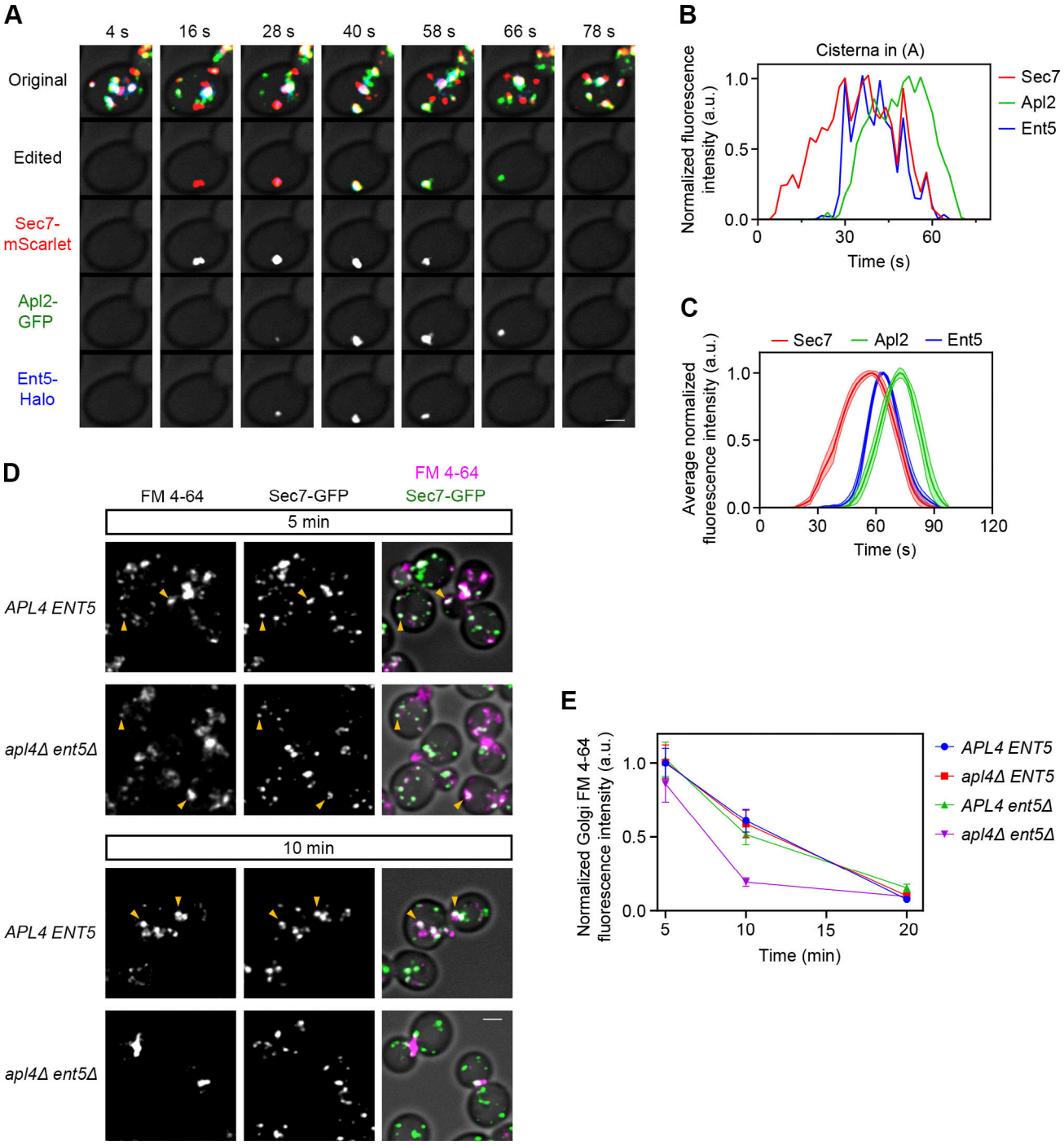

Figure 1. **AP-1 and Ent5 operate at the TGN and are responsible for the persistent TGN localization of internalized FM 4–64. (A)** Maturation kinetics of AP-1 and Ent5 compared with Sec7. A strain expressing the TGN marker Sec7-mScarlet, the AP-1 subunit Apl2-GFP, and the clathrin adaptor Ent5-HaloTag was grown to mid-log phase, labeled with JFX dye, and imaged by 4D confocal microscopy. Shown are average projected Z-stacks at the indicated time points from Video 1. The upper row shows the complete projections, the second row shows edited projections that include only the cisterna being tracked, and the subsequent rows show the individual fluorescence channels from the edited projections. Scale bar, 2 µm. **(B)** Quantification of tagged Golgi proteins during a typical maturation event. Depicted are the normalized fluorescence intensities in arbitrary units for the cisterna tracked in A. **(C)** Smoothed and averaged traces showing the relative kinetic signatures of Sec7, Apl2, and Ent5. Data were obtained for 18 representative cisternae. Lines show mean values, and shaded areas show 95% confidence intervals. **(D)** Comparison of internalized FM 4–64 in *APL4 ENT5* and *apl4Δ ent5Δ* strains. Cells expressing Sec7-GFP were grown to mid–log phase and incubated with FM 4-64FX (a fixable version of FM 4–64) during a 3-min pulse, followed by a chase with the quencher SCAS. Representative images are shown from the 5- and 10-min time points during the chase. Individual fluorescence channels are shown in grayscale with merged images on the right. Arrowheads mark examples of TGN structures that contain FM 4–64. Scale bar, 2 µm. **(E)** Quantification of the analysis in D. For the indicated time points, the Sec7-GFP signals were used to create masks to measure the TGN-associated FM 4–64 fluorescence in *APL4 ENT5*, *apl4Δ ENT5*, *APL4 ent5Δ*, and *apl4Δ ent5Δ* strains. Plotted are the average TGN-associated FM 4–64 signals, normalized to the value in wild-type cells at 5 min. Error bars represent SEM. At least 100 cells of each strain were analyzed per time point.

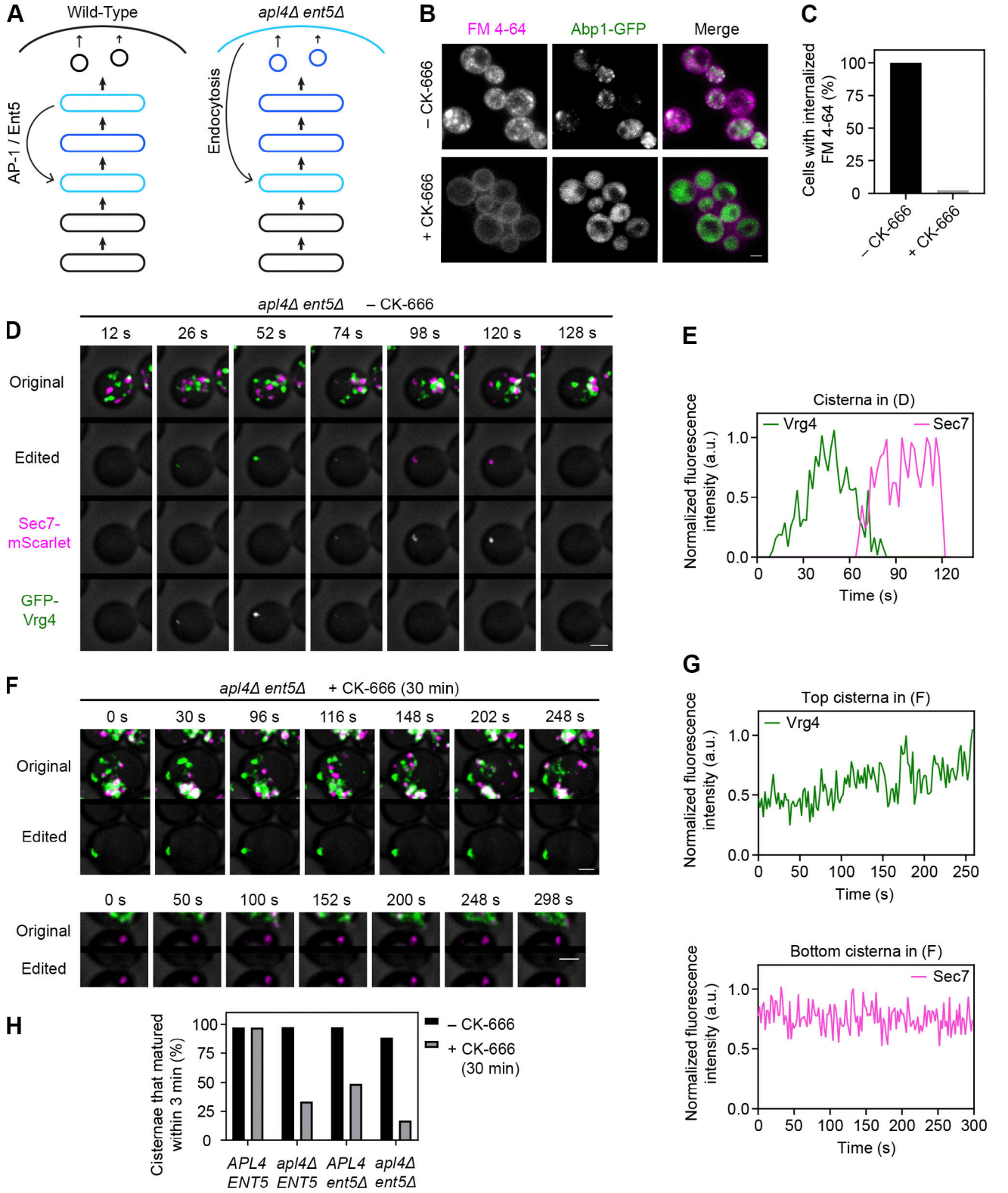

Figure 2. **Inhibition of endocytosis blocks Golgi maturation in cells lacking AP-1/Ent5. (A)** Diagram of the experimental rationale. In wild-type cells, a set of transmembrane TGN proteins, indicated in blue, recycle with the aid of AP-1/Ent5 from terminally maturing TGN cisternae to nascent TGN cisternae. In *apl4Δ ent5Δ* cells, which lack AP-1/Ent5, those TGN proteins presumably reach the plasma membrane in secretory vesicles and then undergo endocytic recycling to nascent TGN cisternae. Inhibition of endocytosis in an *apl4Δ ent5Δ* strain should trap transmembrane TGN proteins in secretory vesicles or at the plasma membrane and should therefore perturb Golgi function. **(B)** Inhibition of endocytosis with CK-666. Cells expressing Abp1-GFP were mock treated or incubated with CK-666 for 15 min, then incubated for 5 min with FM 4-64FX, and then imaged by confocal microscopy. Shown are average projected Z-stacks. Individual fluorescence channels are shown in grayscale with merged images on the right. To preserve diffuse signals, the images were not deconvolved. Scale bar, 2 µm.

(C) Quantification of the analysis in B. Projected images were manually scored for the presence of internalized dye. At least 40 cells were analyzed for each sample. **(D)** A typical Golgi maturation event in an untreated cell lacking AP-1 and Ent5. *apl4Δ ent5Δ* cells expressing the early Golgi marker GFP-Vrg4 and the TGN marker Sec7-mScarlet were grown to mid-log phase and imaged by 4D confocal microscopy. Shown are average projected Z-stacks at the indicated time points from part 1 of Video 2. The upper row shows the complete projections, the second row shows edited projections that include only the cisterna being tracked, and the subsequent rows show the individual fluorescence channels from the edited projections. Scale bar, 2 µm. **(E)** Quantification of the fluorescence signals from the cisterna analyzed in D. **(F)** Persistence of early or TGN markers in cisternae of *apl4Δ ent5Δ* cells after CK-666 treatment. Cells grown to mid-log phase were treated with CK-666 for 30 min before imaging as in D. Shown are average projected Z-stacks at the indicated time points for separate cisternae from Parts 2 and 3 of Video 2. For each analyzed cisterna, the upper row shows the complete projections, and the lower row shows edited projections that include only the cisterna being tracked. Scale bars, 2 µm. **(G)** Quantification of the fluorescence signals from the cisternae analyzed in F. **(H)** Quantification of Golgi maturation events in the absence or presence of CK-666. Cells expressing GFP-Vrg4 and Sec7-mScarlet in the indicated genetic backgrounds were either mock treated or treated with CK-666 for 30 min and were imaged as in D. Individual cisternae were scored according to whether or not they matured within 3 min. At least 36 cisternae from at least 29 cells were analyzed for each strain.

secretion (Finger and Novick, 1998) such as the necks of large-budded cells (Fig. 1 D), suggesting that recycling of FM 4–64 to the cell surface (Wiederkehr et al., 2000) was accelerated in this mutant. Fig. 1 E quantifies FM 4–64 colocalization with Sec7 in the wild-type and double mutant strains and also in the two single mutants. As predicted, FM 4–64 persistence in the TGN was dramatically reduced in the double mutant. These results suggest that AP-1/Ent5 recycles membrane during TGN maturation.

A bypass pathway of recycling from the plasma membrane permits Golgi operation in the absence of AP-1/Ent5

If the AP-1/Ent5 pair plays a major role in intra-Golgi recycling, how do cells survive in the absence of these adaptors? A likely explanation is that in an *apl4Δ ent5Δ* strain, transmembrane proteins that would normally recycle within the Golgi travel instead to the plasma membrane and then recycle to the Golgi by endocytosis (Fig. 2 A). This concept fits with reports that certain TGN proteins could be accumulated at the plasma membrane in AP-1 mutants by blocking endocytosis with the actin polymerization inhibitor latrunculin A (Valdivia et al., 2002; Liu et al., 2008). As a more specific alternative to latrunculin A, we chose CK-666, which inhibits the Arp2/3 complex and selectively prevents endocytosis at actin patches (Hetrick et al., 2013; Burke et al., 2014; Antkowiak et al., 2019). To ensure that CK-666 could act at full potency, the transcription factors Pdr1 and Pdr3 were deleted to prevent expression of pleiotropic drug transporters (Schüller et al., 2007; Barrero et al., 2016). A control experiment confirmed that within minutes after addition, CK-666 redistributed the actin patch component Abp1 (Goode et al., 2001; Huckaba et al., 2004) to the cytosol and completely blocked endocytic internalization of FM 4–64 (Fig. 2, B and C). We therefore predicted that treatment of an *apl4Δ ent5Δ* strain with CK-666 would perturb Golgi function.

Our readout for Golgi function was cisternal maturation, as indicated by conversion of early Golgi cisternae labeled with the GDP-mannose transporter Vrg4 to TGN cisternae labeled with Sec7 (Losev et al., 2006). Normal maturation events were observed in untreated *apl4Δ ent5Δ* cells and in wild-type cells treated with CK-666 (Fig. 2, D, E, and H; and Video 2). However, in *apl4Δ ent5Δ* cells treated with CK-666, cisternal maturation was blocked. Various cisternae showed abnormal persistence of either Vrg4 or Sec7 (Fig. 2, F and G; and Video 2) or more complex patterns that seemed to reflect hybrid or clustered cisternae (unpublished data). These effects are summarized in Fig. 2 H, which quantifies the percentage of cisternae that underwent maturation during a 3-min period. Removal of either AP-1 or Ent5 inhibited maturation in cells treated with CK-666, and this inhibition was nearly complete in cells lacking both adaptors. We conclude that components needed for Golgi operation recycle intracellularly in wild-type cells but recycle via the plasma membrane in *apl4Δ ent5Δ* cells.

A set of transmembrane TGN proteins require AP-1/Ent5 for normal recycling

There is evidence that yeast AP-1 mediates recycling of the TGN-localized phospholipid translocase Drs2 (Liu et al., 2008). AP-1–dependent recycling delivers material when a cisterna is beginning to acquire TGN characteristics (Casler et al., 2019), so we predicted that Drs2 would arrive at a cisterna around the same time as Sec7. This prediction was confirmed by individual and averaged fluorescence traces, which revealed that Drs2 arrived shortly before Sec7 and then departed when AP-1 was present (Fig. 3, A–C; and Video 3).

We tested the idea that in *apl4Δ ent5Δ* cells, Drs2 travels to the plasma membrane in secretory vesicles and then returns to the TGN in endocytic vesicles. Our approach was to inhibit this recycling pathway using CK-666. Two possible outcomes were envisioned. The first possibility is that Drs2 would accumulate at the plasma membrane due to the block in internalization (Liu et al., 2008). The second possibility is that Drs2 would accumulate in secretory vesicles due to slowed fusion of those vesicles with the plasma membrane. This latter scenario is based on the finding that secretion and endocytosis are coupled in yeast (Riezman, 1985; Lewis et al., 2000; Johansen et al., 2016). The two possibilities are not mutually exclusive, and the effects are likely to be partial. Thus, when *apl4Δ ent5Δ* cells are treated with CK-666, some of the Drs2 molecules might be expected to remain in the TGN, but a significant fraction might accumulate at the plasma membrane or in secretory vesicles.

The experimental data matched this prediction. When wild-type cells were treated with CK-666 for 15 min, Drs2 retained its punctate TGN localization (Fig. S1 A), but when *apl4Δ* or *apl4Δ ent5Δ* cells were treated with CK-666, a large fraction of the Drs2 molecules redistributed out of punctate TGN structures (Fig. S2 A and Fig. 3 D). For the CK-666–treated *apl4Δ ent5Δ* strain, some of the cells showed Drs2 in a diffuse pattern consistent with plasma membrane localization, while other cells showed Drs2 at

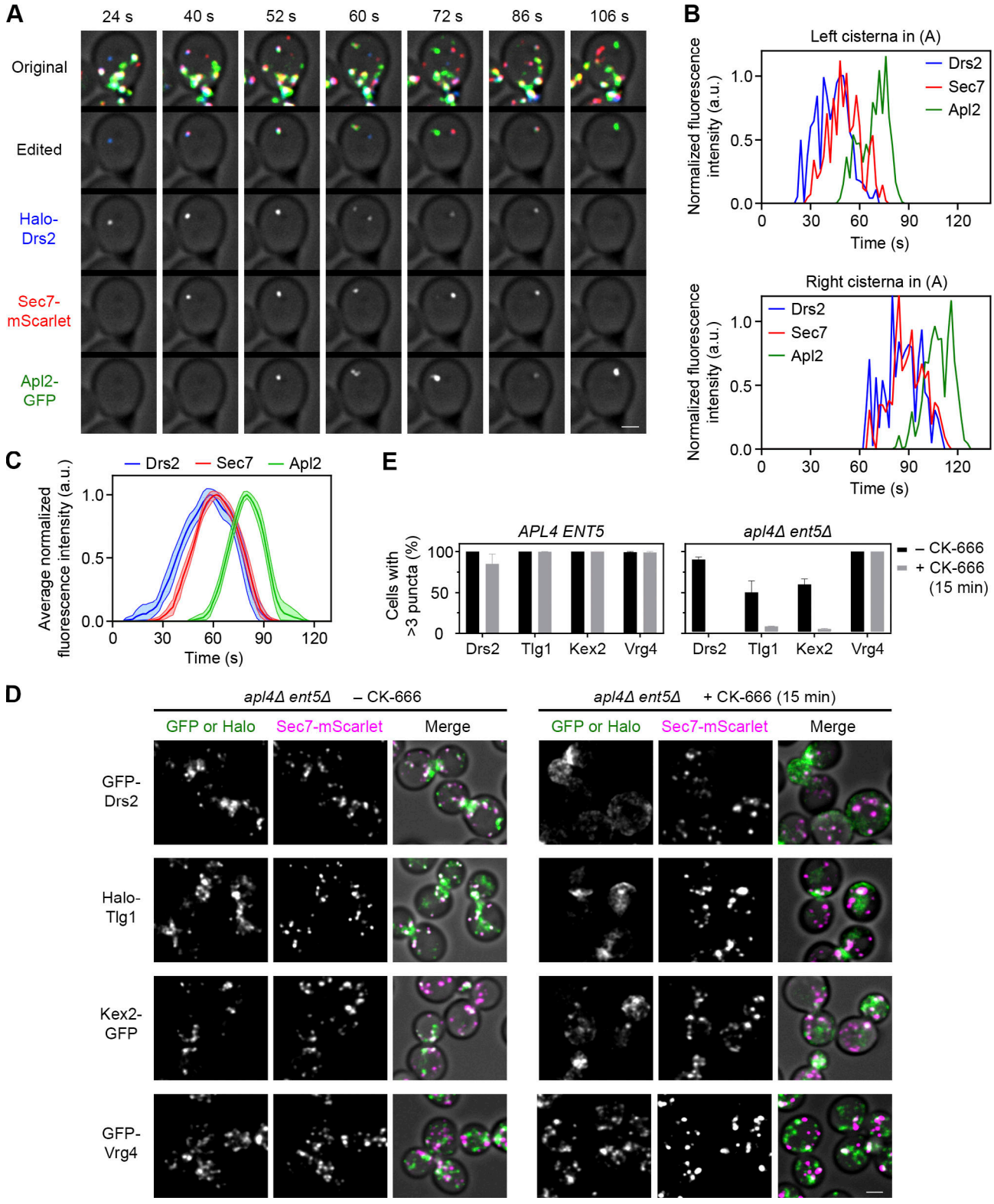

Figure 3. **Drs2 and other transmembrane TGN proteins localize with the aid of AP-1/Ent5. (A)** Maturation kinetics of Drs2 compared with Sec7 and AP-1. A strain expressing the TGN marker Sec7-mScarlet, the AP-1 subunit Apl2-GFP, and HaloTag-Drs2 was grown to mid-log phase, labeled with JFX dye, and imaged by 4D confocal microscopy. Shown are average projected Z-stacks at the indicated time points from Video 3. The upper row shows the complete projections, the second row shows edited projections that include only the cisternae being tracked, and the subsequent rows show the individual fluorescence channels from the edited projections. Two events are shown. Scale bar, 2 µm. **(B)** Quantification of tagged Golgi proteins during typical maturation events. Depicted are the normalized fluorescence intensities in arbitrary units for the cisternae tracked in A. **(C)** Smoothed and averaged traces showing the relative kinetic signatures of Drs2, Sec7, and Apl2. Data were obtained for 17 representative cisternae. **(D)** Mislocalization of transmembrane TGN proteins in *apl4Δ*

ent5Δ cells after CK-666 treatment. *apl4Δ ent5Δ* cells expressing Sec7-mScarlet and the indicated HaloTag- or GFP-tagged Golgi protein were grown to mid-log phase and then imaged by confocal microscopy 15 min after mock treatment or treatment with CK-666. Shown are average projected Z-stacks. Individual fluorescence channels are shown in grayscale with merged images on the right. Scale bar, 2 µm. **(E)** Quantification of the effects of the procedure in D for *APL4 ENT5* and *apl4Δ ent5Δ* cells. For a given cell, the individual slices in a Z-stack were examined in the GFP or HaloTag channel to determine whether the cell contained three or more punctate structures with the shape and size characteristics of Golgi cisternae. Each bar represents an average of two biological replicates in which at least 40 cells were scored per condition. Error bars represent SEM.

sites of polarized secretion in a pattern consistent with secretory vesicle localization (Finger and Novick, 1998). We found that this partial redistribution out of Golgi compartments could be quantified by counting the percentage of cells in which Drs2 was visible in more than three punctate structures (Fig. 3 E). As a control, Vrg4 recycles in the early Golgi with the aid of COPI (Abe et al., 2004; Papanikou et al., 2015), and its distribution in either wild-type or *apl4Δ ent5Δ* cells was unaffected by CK-666 (Fig. S1 B; and Fig. 3, D and E). Thus, CK-666 treatment of *apl4Δ ent5Δ* cells seems to be a suitable test of whether a transmembrane Golgi protein recycles with the aid of AP-1/Ent5.

This test was applied to several transmembrane TGN proteins that colocalized extensively with Sec7 (Fig. S1 A). A functional study implicated AP-1 in TGN localization of the SNARE protein Tlg1 (Valdivia et al., 2002). Indeed, when *apl4Δ ent5Δ* cells were treated with CK-666, Tlg1 showed a reduced punctate distribution and was often concentrated at sites of polarized secretion (Fig. 3, D and E). The next candidate was the processing protease Kex2 (Fuller et al., 1988). It has long been thought that Kex2 recycles via PVE compartments, but the evidence is ambiguous (see Discussion), and we have proposed instead that Kex2 follows an intra-Golgi recycling pathway (Papanikou et al., 2015). When *apl4Δ ent5Δ* cells were treated with CK-666, Kex2 showed a reduced punctate distribution and was often concentrated at sites of polarized secretion (Fig. 3, D and E), suggesting that AP-1/Ent5–dependent recycling is the primary localization mechanism for Kex2. Similar results were obtained with two other transmembrane Golgi proteins: Ste13, which is a dipeptidyl aminopeptidase that acts downstream of Kex2 (Fuller et al., 1988), and Stv1, which is a component of the TGN-localized proton-pumping ATPase (Manolson et al., 1994; Finnigan et al., 2012; Fig. S3 A). In wild-type cells, as expected, CK-666 had no effect on the punctate TGN localizations of Tlg1, Kex2, Ste13, or Stv1 (Fig. S1 A). Further control experiments confirmed that the early Golgi glycosylation enzymes Anp1 and Mnn9 (Jungmann and Munro, 1998) resembled Vrg4 in being unaffected by CK-666 in either wild-type or *apl4Δ ent5Δ* cells (Fig. S1 B and Fig. S3 B). Prior to CK-666 treatment, *apl4Δ ent5Δ* cells showed reduced TGN labeling for Drs2, Tlg1, Kex2, Ste13, and Stv1—presumably because some of the protein molecules were recycling between the TGN and plasma membrane at steady state—whereas no such effect was seen for Vrg4, Anp1, or Mnn9 (Fig. S3, A and B; and unpublished data). Thus, AP-1/Ent5 specifically mediates recycling of a set of transmembrane TGN proteins.

These TGN proteins did exhibit some differences in their responses. After CK-666 treatment, Drs2 was more likely than the other proteins to show a diffuse pattern in an *apl4Δ ent5Δ* strain (Fig. 3 D), and Drs2 uniquely showed extensive redistribution out of TGN structures in either an *apl4Δ* strain or an *ent5Δ* strain (Fig. S2, A and B; and Fig. S3 A). In an *ent5Δ* strain but not in an *apl4Δ* strain, Tlg1 showed decreased TGN localization in untreated cells (Hung and Duncan, 2016) and loss of TGN localization in CK-666–treated cells (Fig. S2, A and B; and Fig. S3 A). Despite these variations, the basic result is that removal of AP-1/Ent5 alters the trafficking of multiple transmembrane TGN proteins.

Removal of AP-1/Ent5 diverts Kex2 to a plasma membrane recycling pathway

The results obtained with *apl4Δ ent5Δ* cells suggest that removal of AP-1/Ent5 causes multiple TGN proteins to be packaged into secretory vesicles. We tested this interpretation in two ways, in each case by using Kex2 as a representative TGN protein.

First, in *apl4Δ ent5Δ* cells, Kex2 should remain in the TGN until the cisternae mature to form secretory vesicles. This prediction was tested by tracking Kex2 together with Sec7, which departs at approximately the same time as a secretory cargo (Casler et al., 2019). Sec7 normally persists longer than Kex2 (Papanikou et al., 2015). Averaging of fluorescence traces revealed that in wild-type cells, Kex2 typically departed ∼15 s before Sec7 (Fig. 4, A–C; and Video 4). In *apl4Δ ent5Δ* cells, the data were noisy because the Golgi signal for Kex2 was reduced in the absence of AP-1/Ent5, but Kex2 persisted for as long as Sec7, presumably because Kex2 remained in the cisternae until being packaged into secretory vesicles (Fig. 4, D–F; and Video 4). This result matches the prediction.

Second, as described above, if endocytosis is blocked in *apl4Δ ent5Δ* cells, then AP-1/Ent5–dependent TGN proteins such as Kex2 might accumulate in secretory vesicles. This prediction fits with the finding that CK-666 treatment of *apl4Δ ent5Δ* cells redistributed multiple TGN proteins to sites of polarized secretion. To characterize this effect, we marked secretory vesicles with tagged Sec2, which is recruited to terminally maturing cisternae as they transform into secretory vesicles (Elkind et al., 2000; Mizuno-Yamasaki et al., 2010). Sec2 was often found where secretory vesicles accumulate, either in small or nascent buds or at the necks of large-budded cells (Fig. 4 G). In CK-666–treated wild-type cells, Kex2 did not colocalize with Sec2, whereas in CK-666–treated *apl4Δ ent5Δ* cells, Kex2 colocalized with Sec2 ∼95% of the time. Two particularly clear examples of this colocalization are shown in Fig. 4 G, and quantification of the data is described in the figure legend. The combined results support the conclusion that removal of AP-1/Ent5 diverts Kex2 into secretory vesicles.

AP-1/Ent5–dependent TGN proteins show similar kinetic signatures

We compared the kinetic signatures of the AP-1/Ent5–dependent Tlg1, Kex2, Ste13, and Stv1 proteins to that of Drs2 during Golgi

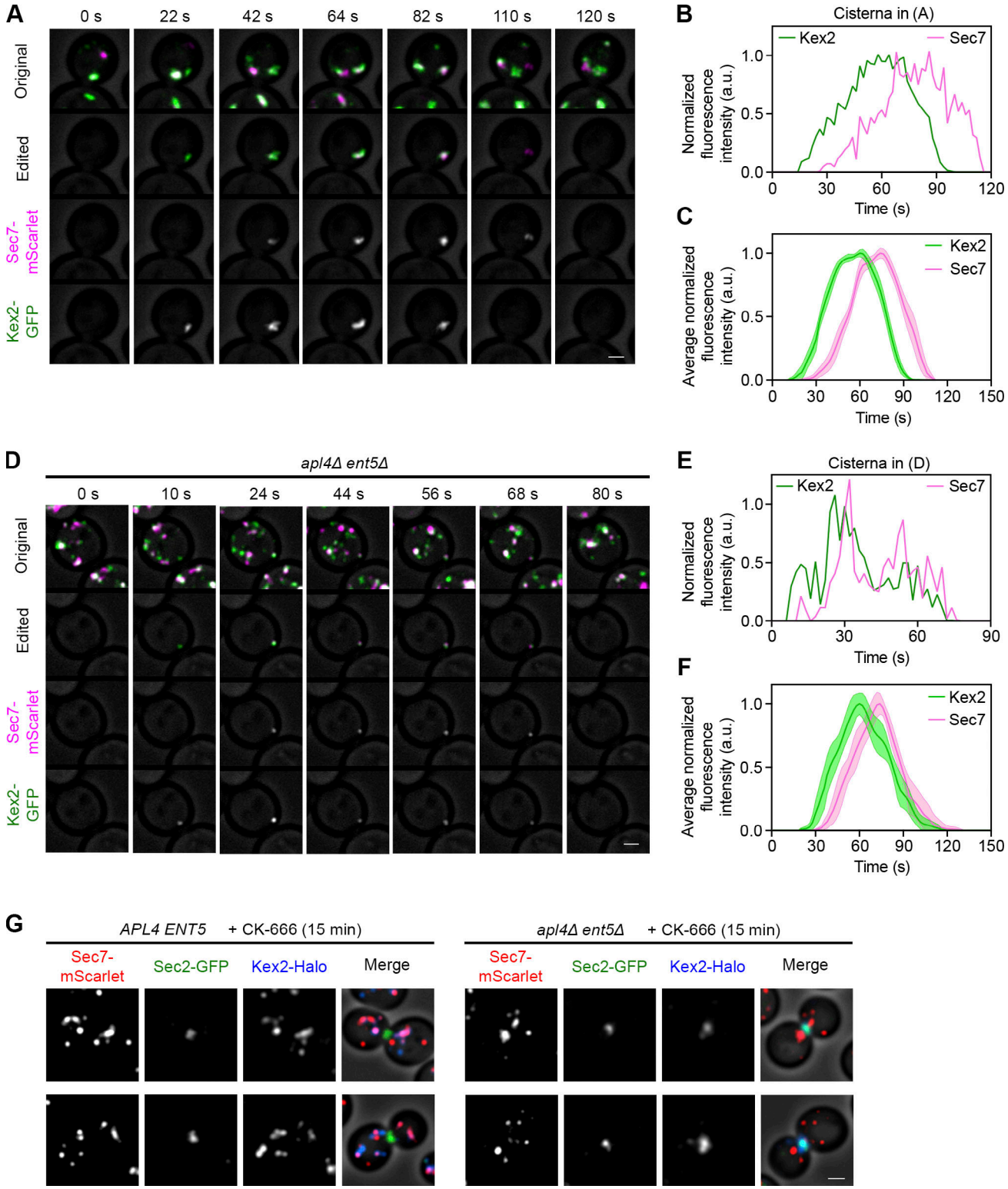

Figure 4. **Removal of AP-1/Ent5 causes Kex2 to enter secretory vesicles. (A)** Maturation kinetics of Kex2 compared with Sec7. A strain expressing Sec7-mScarlet and the processing protease Kex2-GFP was grown to mid-log phase and imaged by 4D confocal microscopy. Shown are average projected Z-stacks at the indicated time points from part 1 of Video 4. The upper row shows the complete projections, the second row shows edited projections that include only the cisterna being tracked, and the subsequent rows show the individual fluorescence channels from the edited projections. Scale bar, 2 µm. **(B)** Quantification of tagged Golgi proteins during a typical maturation event. Depicted are the normalized fluorescence intensities in arbitrary units for the cisterna tracked in A. **(C)** Smoothed and averaged traces showing the relative kinetic signatures of Kex2 and Sec7. Data were obtained for 10 representative cisternae. **(D)** Maturation kinetics of Kex2 compared with Sec7 in an *apl4Δ ent5Δ* strain. The experiment was performed as in A. Shown are average projected Z-stacks at the indicated time points from part 2 of Video 4. Scale bar, 2 µm. **(E)** Quantification of tagged Golgi proteins during a typical maturation event in an *apl4Δ ent5Δ*

strain. Depicted are the normalized fluorescence intensities in arbitrary units for the cisterna tracked in D. **(F)** Smoothed and averaged traces showing the relative kinetic signatures of Kex2 and Sec7 in an *apl4Δ ent5Δ* strain. Data were obtained for 10 representative cisternae. **(G)** Localization of Kex2 to sites of polarized secretion in *apl4Δ ent5Δ* cells after CK-666 treatment. *APL4 ENT5* or *apl4Δ ent5Δ* cells expressing Sec7-mScarlet, Sec2-GFP, and Kex2-HaloTag were grown to mid-log phase, labeled with JFX dye, and imaged by confocal microscopy 15 min after treatment with CK-666. Shown are average projected Z-stacks. Individual fluorescence channels are shown in grayscale with merged images on the right. The pair of budded cells of the *APL4 ENT5* strain is typical for the population, while the pair of budded cells of the *apl4Δ ent5Δ* strain is a striking example that illustrates the population trend. Scale bar, 2 µm. Quantification of the projected images was performed with the 60–75% of the cells in which Sec2 was concentrated at the bud neck or in a small or nascent bud. Approximately 10–20% of those cells were excluded from further consideration because they showed Sec7-labeled TGN structures in close proximity to Sec2. For the *APL4 ENT5* strain, 109 cells were deemed suitable for analysis, and Kex2 overlapped with Sec2 in none (0%) of those cells. For the *apl4Δ ent5Δ* strain, 153 cells were deemed suitable for analysis, and Kex2 overlapped with Sec2 in 145 (95%) of those cells.

maturation (Fig. 5, A–F; Fig. S4, A–F; and Video 4). All four TGN proteins resembled Drs2 in their kinetic signatures. Drs2 tended to persist ∼5–15 s longer than the other TGN proteins, but those differences were minor. By contrast, the AP-1/Ent5–independent early Golgi proteins Vrg4, Anp1, and Mnn9 arrived and departed ∼60 s earlier than Drs2 (Fig. 5, G–I; Fig. S5; and Video 5). These data support the assignment of Drs2, Tlg1, Kex2, Ste13, and Stv1 to a kinetic class that reflects their recycling pathway.

TGN proteins that recycle via PVE compartments depart much sooner than Drs2 and localize independently of AP-1/Ent5

Some transmembrane TGN proteins, such as the vacuolar hydrolase receptor Vps10, travel to PVE compartments and then recycle to the Golgi (Marcusson et al., 1994; Cooper and Stevens, 1996). Vps10 is packaged into Golgi-derived vesicles with the aid of the GGA clathrin adaptors (Black and Pelham, 2000; Dell'Angelica et al., 2000; Hirst et al., 2000; Zhdankina et al., 2001), which arrive before AP-1 and Ent5 (Daboussi et al., 2012; Casler and Glick, 2020). We showed recently that a Vps10-dependent biosynthetic cargo begins to exit the Golgi immediately after a cisterna acquires TGN characteristics (Casler and Glick, 2020). Vps10 would therefore be expected to depart from TGN cisternae well before Drs2. Indeed, the kinetic signatures of Vps10 and Drs2 were quite different (Fig. 6, A–C; and Video 6). Vps10 always arrived before Drs2, with a typical offset of ∼6–7 s, and then began to depart while Drs2 levels were still increasing. As a second example of a TGN protein that likely recycles via PVE compartments, we examined the Na^+/H^+ exchanger Nhx1, which resembles Vps10 in showing dual localization to TGN and PVE structures (Kojima et al., 2012; Chi et al., 2014; Papanikou et al., 2015). The fluorescence signals for Nhx1 were relatively weak, but we found that the kinetic signature of Nhx1 was similar to that of Vps10 and clearly distinct from that of Drs2 (Fig. 6, D–F; and Video 6). Thus, Vps10 and Nhx1 can be assigned to a second kinetic class of transmembrane TGN proteins.

Because Vps10 exits the Golgi in GGA-dependent carriers, its intracellular distribution should be unaffected by removal of AP-1/Ent5. As predicted, when *apl4Δ ent5Δ* cells were treated with CK-666, Vps10 showed no loss of punctate localization (Fig. 6, G and H). Similar results were obtained for Nhx1 (Fig. 6, G and H). The localization of Vps10 and Nhx1 to both TGN and PVE structures was similar in wild-type and *apl4Δ ent5Δ* cells (Fig. 6 G and unpublished data). We conclude that Vps10 and Nhx1 recycle in a manner independent of AP-1/Ent5. These findings bolster the argument that the kinetic signatures of Golgi transmembrane proteins reflect their recycling pathways.

A class of AP-1/Ent5–dependent Golgi proteins have intermediate residence times

We were curious about the transmembrane protein Sys1, which initiates the process of recruiting the Arl1 GTPase (Behnia et al., 2004; Setty et al., 2004). Our original analysis suggested that Sys1 and Sec7 had similar kinetic signatures (Losev et al., 2006), but for that experiment Sys1 was overexpressed, and later studies from the Nakano group reported that Sys1 arrives and departs well before Sec7 (Ishii et al., 2016; Kurokawa et al., 2019; Tojima et al., 2019). Fig. 7, A–C, and Video 7 confirm the distinct kinetic signatures of Sys1 and Sec7 and also provide a comparison with Drs2. On average, Sys1 arrived and departed ∼15–20 s before Drs2. Sys1 therefore defines an additional kinetic class of transmembrane Golgi proteins.

Unexpectedly, when *apl4Δ ent5Δ* cells were treated with CK-666, the punctate Golgi signal for Sys1 became less prominent, and Sys1 showed frequent colocalization with the secretory vesicle marker Sec2 (Fig. 7, D and E). This effect was seen only upon removal of both AP-1 and Ent5 (Fig. 7 E). The implication is that in the absence of AP-1/Ent5, Sys1 switches to the bypass recycling pathway of transit to the plasma membrane followed by endocytosis. We tested this idea by examining the kinetic signature of Sys1 in *apl4Δ ent5Δ* cells. The data were noisy because the Golgi signal for Sys1 was reduced in the absence of AP-1/Ent5, but there was a major shift that brought the Sys1 kinetic signature much closer to that of Sec7 (Fig. 7, F–H; and Video 7). Quantification of the averaged data revealed that in wild-type cells, Sys1 arrived ∼25 s before Sec7 and departed ∼19 s before Sec7, whereas in *apl4Δ ent5Δ* cells, Sys1 arrived ∼7 s before Sec7 and departed at the same time as Sec7. In *apl4Δ ent5Δ* cells, the kinetic signature of Sys1 (Fig. 7 H) resembled that of Kex2 (see Fig. 4 F), suggesting that both proteins were diverted to the same pathway of delivery to the plasma membrane followed by endocytosis. A plausible interpretation is that AP-1/Ent5 mediates a second intra-Golgi recycling pathway that causes Sys1 to reside in cisternae during an intermediate phase of maturation.

Do other transmembrane Golgi proteins recycle in the same manner as Sys1? We examined Golgi proteins that have been described as having neither early nor TGN localizations. One candidate was Aur1, an inositol phosphorylceramide synthase (Nagiec et al., 1997; Levine et al., 2000). Aur1 reportedly shows partial colocalization with early and TGN markers (Levine et al., 2000). Another candidate was Rbd2, a putative rhomboid protease that also shows partial colocalization with early and TGN markers (Cortesio et al., 2015; Lastun et al., 2016). We found that both Aur1 and Rbd2 had kinetic signatures resembling that of Sys1 (Fig. 8, C–H; and Video 8). Moreover, both proteins partially

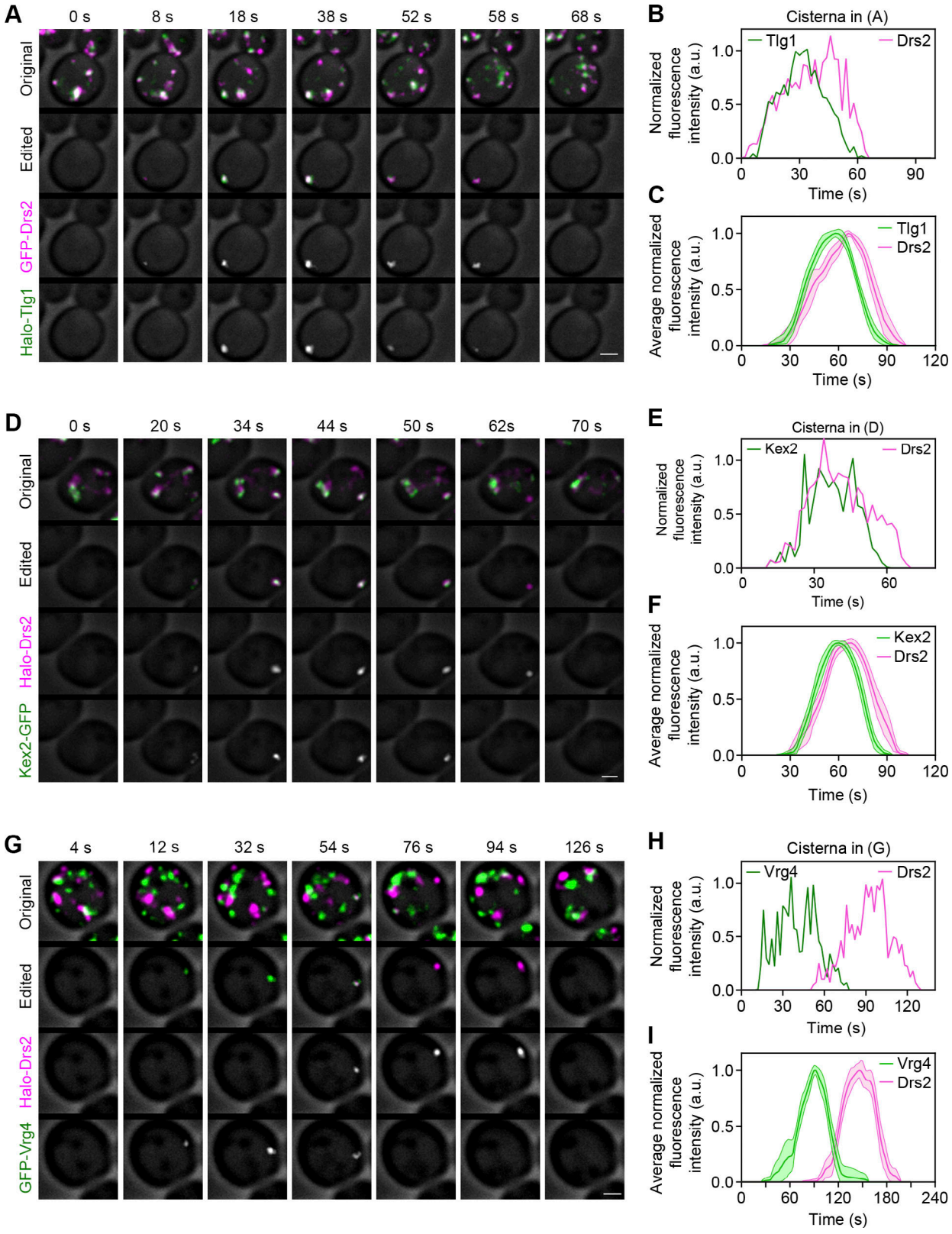

Figure 5. **Other transmembrane TGN proteins resemble Drs2 in their kinetic signatures. (A)** Maturation kinetics of Drs2 compared with Tlg1. A strain expressing GFP-Drs2 and the SNARE HaloTag-Tlg1 was grown to mid-log phase, labeled with JFX dye, and imaged by 4D confocal microscopy. Shown are average projected Z-stacks at the indicated time points from part 3 of Video 4. The upper row shows the complete projections, the second row shows edited projections that include only the cisterna being tracked, and the subsequent rows show the individual fluorescence channels from the edited projections. Scale bar, 2 µm. **(B)** Quantification of tagged Golgi proteins during a typical maturation event. Depicted are the normalized fluorescence intensities in arbitrary units for the cisterna tracked in A. **(C)** Smoothed and averaged traces showing the relative kinetic signatures of Drs2 and Tlg1. Data were obtained for 10

representative cisternae. **(D)** Maturation kinetics of Drs2 compared with Kex2. The experiment was performed as in A, except with a strain expressing HaloTag-Drs2 and Kex2-GFP. Shown are average projected Z-stacks at the indicated time points from part 4 of Video 4. Scale bar, 2 µm. **(E)** Quantification of tagged Golgi proteins during a typical maturation event. Depicted are the normalized fluorescence intensities in arbitrary units for the cisterna tracked in D. **(F)** Smoothed and averaged traces showing the relative kinetic signatures of Drs2 and Kex2. Data were obtained for 13 representative cisternae. **(G)** Maturation kinetics of Drs2 compared with Vrg4. The experiment was performed as in A, except with a strain expressing HaloTag-Drs2 and GFP-Vrg4. Shown are average projected Z-stacks at the indicated time points from part 1 of Video 5. Scale bar, 2 µm. **(H)** Quantification of tagged Golgi proteins during a typical maturation event. Depicted are the normalized fluorescence intensities in arbitrary units for the cisterna tracked in G. **(I)** Smoothed and averaged traces showing the relative kinetic signatures of Drs2 and Vrg4. Data were obtained for 12 representative cisternae.

redistributed out of punctate Golgi structures when *apl4Δ ent5Δ* cells were treated with CK-666 (Fig. 8, A and B). The loss of Golgi localization was less extensive for Aur1 and Rbd2 (Fig. 8 B) than for the transmembrane TGN proteins examined earlier (see Fig. S3 A), but the effect was clear. Therefore, AP-1/Ent5 is involved in recycling not only TGN proteins but also a class of transmembrane proteins that would traditionally be said to reside in the medial/trans Golgi.

Discussion

When yeast cells are examined using static images, Golgi proteins often colocalize with one another in some cisternae but not in others. Therefore, as with mammalian cells, rigorous definitions of yeast Golgi compartments have been elusive. We suggest that a more natural way to characterize the Golgi is kinetic analysis. The key factor is recycling pathways: for a given transmembrane Golgi protein, the recycling pathway determines when that protein resides in a maturing cisterna (Pantazopoulou and Glick, 2019). Each recycling pathway has a unique kinetic signature that defines a class of transmembrane Golgi proteins (Fig. 9 A).

This view has now been validated by identifying multiple recycling pathways for the yeast Golgi. One pathway, not examined here, is COPI-dependent transport from the Golgi to the ER followed by recycling to the early Golgi (Gaynor et al., 1998; Barlowe and Miller, 2013). A second pathway is COPI-dependent recycling within the early Golgi of proteins such as Vrg4 (Papanikou et al., 2015; Fig. 9 B). A third pathway involves AP-1. Functional studies originally suggested that yeast AP-1 recycles transmembrane proteins from early endosomes to the TGN (Valdivia et al., 2002; Foote and Nothwehr, 2006; Liu et al., 2008; Spang, 2015). However, yeast early endosomes are identical to the TGN, and AP-1 localizes exclusively to maturing TGN cisternae, implying that AP-1 actually mediates intra-Golgi recycling of TGN proteins (Day et al., 2018). An example of an AP-1–dependent TGN protein is Drs2 (Liu et al., 2008). We show here that Drs2 departs from maturing cisternae after AP-1 appears and then arrives at younger cisternae shortly before the early-to-TGN transition. The combined results imply that AP-1 mediates intra-Golgi recycling of Drs2 downstream of COPI (Papanikou et al., 2015; Day et al., 2018; Casler et al., 2019).

A well-characterized TGN protein is Kex2 (Fuller et al., 1988). Our earlier video microscopy studies (Papanikou et al., 2015) were extended here by showing that the kinetic signature of Kex2 resembles that of Drs2. To test whether Kex2 relies on AP-1 for its localization, we built on a previously described strategy (Valdivia et al., 2002; Liu et al., 2008). The rationale is that if AP-1 mediates recycling of a Golgi protein, then removal of AP-1 should divert that Golgi protein to a pathway of delivery to the plasma membrane followed by endocytosis. We optimized a procedure for specifically inhibiting endocytosis by using CK-666 to block formation of branched actin (Hetrick et al., 2013; Burke et al., 2014; Antkowiak et al., 2019). In cells lacking AP-1, CK-666 trapped Drs2 at the plasma membrane or in secretory vesicles, consistent with a published report (Liu et al., 2008). However, we did not see a similar effect for Kex2. One possible explanation is that in addition to AP-1, another recycling factor might operate at the TGN.

The epsin-related adaptors Ent3, Ent4, and Ent5 localize to the yeast TGN (Myers and Payne, 2013). Little is known about Ent4 (Deng et al., 2009). Ent3 appears to act early in TGN maturation together with GGAs (Costaguta et al., 2006; Čopič et al., 2007; Daboussi et al., 2012). Ent5 also interacts with GGAs, but the primary role of Ent5 seems to be later in TGN maturation, when it acts together with AP-1 (Costaguta et al., 2006; Čopič et al., 2007; Daboussi et al., 2012; Hung and Duncan, 2016). We therefore tested whether the AP-1/Ent5 pair mediates intra-Golgi recycling. Indeed, in cells lacking AP-1/Ent5, CK-666 caused extensive redistribution of Kex2 and several other TGN proteins out of Golgi structures. No such effect was seen for early Golgi proteins or for Golgi proteins that recycle from PVE compartments. The implication is that in the mutant cells, proteins that would normally recycle with the aid of AP-1/Ent5 travel instead to the plasma membrane and then return to the Golgi by endocytosis. Thus, CK-666 treatment of cells lacking AP-1 and Ent5 is a convenient way to determine whether a given transmembrane Golgi protein undergoes AP-1/Ent5–dependent recycling.

We predicted that the AP-1/Ent5–dependent TGN proteins would all have similar kinetic signatures. This prediction was largely confirmed. Drs2 tended to depart somewhat later during maturation than other TGN proteins, suggesting that there is variation in the process of packaging into AP-1/Ent5 vesicles. But overall, the AP-1/Ent5–dependent class of TGN proteins showed only small differences in their kinetic signatures (Fig. 9 B), consistent with the idea that the recycling pathway determines when a transmembrane Golgi protein is present in maturing cisternae.

Further support for this concept came from examining TGN proteins that follow a different recycling pathway. Vps10 undergoes GGA-dependent traffic from the TGN to PVE compartments followed by recycling to the Golgi (Marcusson et al., 1994; Cooper and Stevens, 1996), so Vps10 is found both in the TGN and in PVE compartments (Chi et al., 2014; Papanikou et al., 2015). As expected, Vps10 localization is unperturbed when cells lacking AP-1/Ent5 are treated with CK-666. Vps10

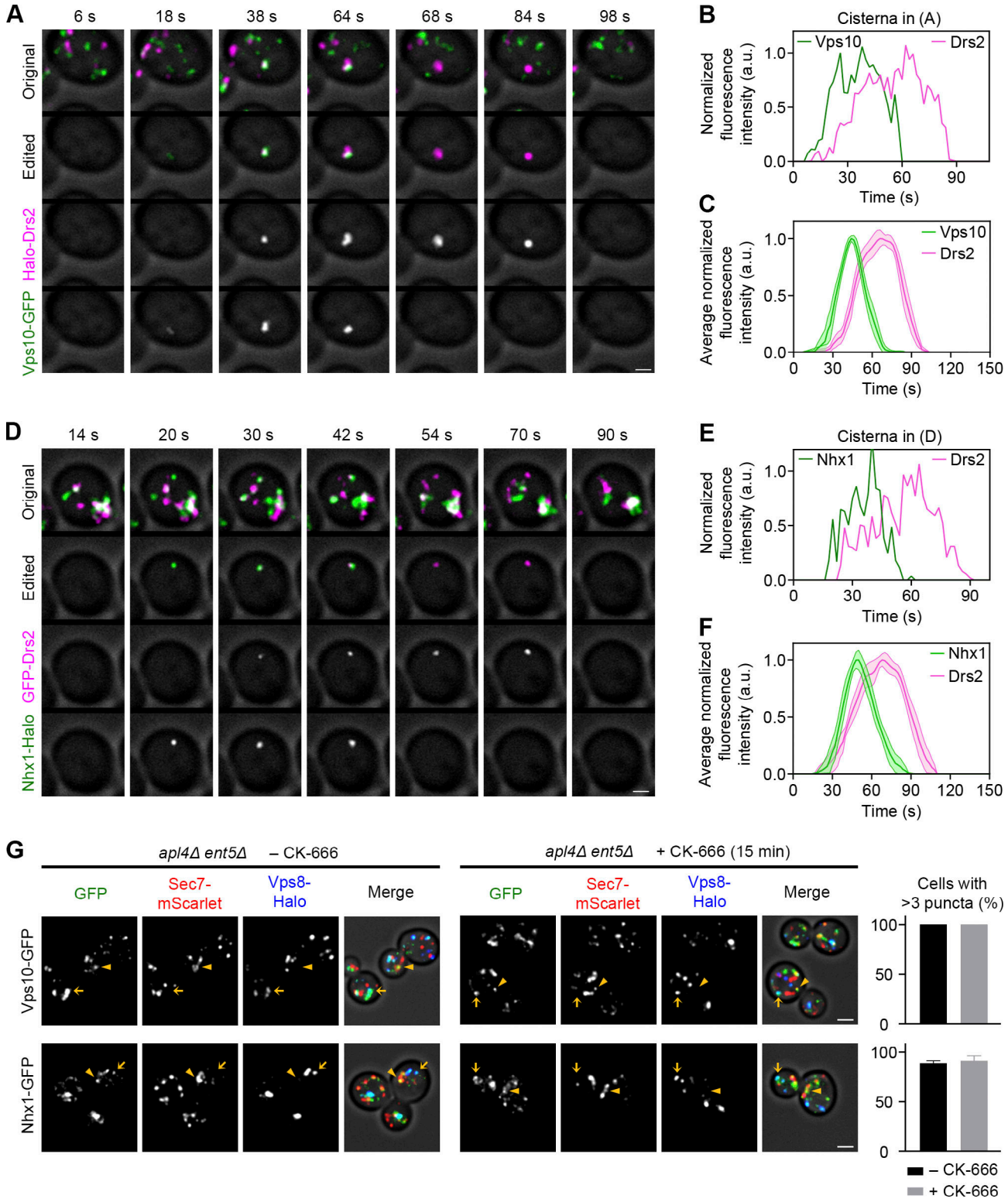

Figure 6. **A separate class of transmembrane TGN proteins recycle via PVE compartments. (A)** Maturation kinetics of Drs2 compared with Vps10. A strain expressing HaloTag-Drs2 and the vacuolar hydrolase receptor Vps10-GFP was grown to mid-log phase, labeled with JFX dye, and imaged by 4D confocal microscopy. Shown are average projected Z-stacks at the indicated time points from part 1 of Video 6. The upper row shows the complete projections, the second row shows edited projections that include only the cisterna being tracked, and the subsequent rows show the individual fluorescence channels from the edited projections. Scale bar, 2 µm. **(B)** Quantification of tagged Golgi proteins during a typical maturation event. Depicted are the normalized fluorescence intensities in arbitrary units for the cisterna tracked in A. **(C)** Smoothed and averaged traces showing the relative kinetic signatures of Drs2 and Vps10. Data were obtained for 15 representative cisternae. **(D)** Maturation kinetics of Drs2 compared with Nhx1. The experiment was performed as in A, except with a strain expressing GFP-Drs2 and the Na^+/H^+ exchanger Nhx1-HaloTag. Shown are average projected Z-stacks at the indicated time points from part 2 of Video

6. Scale bar, 2 µm. **(E)** Quantification of tagged Golgi proteins during a typical maturation event. Depicted are the normalized fluorescence intensities in arbitrary units for the cisterna tracked in D. **(F)** Smoothed and averaged traces showing the relative kinetic signatures of Drs2 and Nhx1. Data were obtained for eight representative cisternae. **(G)** Dual localization of Vps10 and Nhx1 before and after treatment with CK-666. *apl4Δ ent5Δ* strains expressing the TGN marker Sec7-mScarlet, the PVE compartment marker Vps8-HaloTag, and either Vps10-GFP or Nhx1-GFP were grown to mid-log phase, labeled with JFX dye, and imaged by 4D confocal microscopy 15 min after mock treatment or treatment with CK-666. Shown are average projected Z-stacks. Individual fluorescence channels are shown in grayscale with merged images on the right. Arrowheads mark examples of Sec7-labeled TGN structures that contain Vps10 or Nhx1, and arrows mark examples of Vps8-labeled PVE compartments that contain Vps10 or Nhx1. Scale bar, 2 µm. At the right, the same *apl4Δ ent5Δ* strains were treated with CK-666 and manually scored for the presence of three or more punctate spots in the GFP channel, as in Fig. 3 E. Error bars represent SEM.

resembles a previously characterized Vps10-dependent cargo (Casler and Glick, 2020) in departing to PVE compartments soon after the early-to-TGN transition. Because Vps10 arrives at cisternae just before the early-to-TGN transition, this protein has a relatively short residence time during cisternal maturation. The kinetic signature of Vps10 overlaps with that of Drs2 (orange versus blue curves in Fig. 9 A), but Vps10 departs earlier than Drs2 because GGAs act before AP-1/Ent5 (Daboussi et al., 2012; Casler and Glick, 2020). Similar results were obtained for Nhx1, which is also believed to cycle between the TGN and PVE compartments (Kojima et al., 2012). Therefore, we can differentiate between two classes of TGN proteins based on their recycling pathways and kinetic signatures (Fig. 9 B).

The assignment of Kex2 to a different class of TGN proteins than Vps10 was not obvious because, for many years, Kex2 has been assumed to recycle from PVE compartments. As evidence for that view, when mutations were used to block PVE-to-Golgi recycling, Kex2 accumulated in PVE compartments and the vacuole (Wilcox et al., 1992; Voos and Stevens, 1998). But those results are potentially misleading because if Kex2 visits PVE compartments only occasionally, a block in recycling will still trap most of the Kex2 molecules in PVE compartments. Unlike Vps10, Kex2 has no known function in PVE compartments and is present at very low concentrations in PVE compartments, suggesting that the main pathway for Kex2 localization might be recycling within the TGN (Papanikou et al., 2015; Day et al., 2018). Similar arguments hold for Ste13, a TGN protein that acts after Kex2 (Fuller et al., 1988). Ste13 has also been assumed to recycle from PVE compartments, and the signals and mechanisms for retrieving Ste13 from PVE compartments have been studied (Voos and Stevens, 1998; Nothwehr et al., 2000; Harrison et al., 2014; Ma and Burd, 2020). Yet our analysis classifies Ste13 together with Kex2 as an AP-1/Ent5–dependent TGN protein. An elegant pair of earlier reports showed that the transit of Ste13 to PVE compartments is slow, with a half-time of ∼60 min, and that a fast-acting AP-1–dependent process keeps Ste13 in the TGN (Bryant and Stevens, 1997; Foote and Nothwehr, 2006). In our view, proteins such as Kex2 and Ste13 normally recycle within the TGN by an AP-1/Ent5–dependent pathway, but they sometimes escape to PVE compartments, where a salvage pathway returns them to the TGN.

More generally, salvage pathways probably play an important role at the Golgi. Transmembrane Golgi proteins recycle on a time scale of minutes, so occasional missorting in the absence of a corrective mechanism would quickly deplete those proteins from their normal locations. The efficient endocytosis of TGN proteins in cells lacking AP-1/Ent5 may reflect the action of a salvage pathway that operates in wild-type cells to retrieve missorted TGN proteins from the plasma membrane.

The hypothesis that COPI recycles early Golgi proteins while AP-1/Ent5 recycles many TGN proteins does not account for Sys1, which has an intermediate kinetic signature (Ishii et al., 2016; Kurokawa et al., 2019; Tojima et al., 2019). We verified that Sys1 arrives and departs earlier than Drs2 and other TGN proteins (Fig. 9 B). Remarkably, in cells lacking AP-1/Ent5, CK-666 caused extensive redistribution of Sys1 out of Golgi structures. Similar results were observed for additional proteins with intermediate kinetic signatures (Fig. 9 B). We infer that AP-1/Ent5 participates in the recycling of two classes of Golgi proteins by two kinetically distinct pathways.

A simple explanation would be that one class of Golgi proteins is recycled by AP-1 and the other by Ent5, but for most of the Golgi proteins tested, CK-666 had little effect in cells singly lacking either AP-1 or Ent5. AP-1 and Ent5 are at least partially independent in their actions (Costaguta et al., 2006; Čopič et al., 2007), and Ent5 departs from the TGN sooner than AP-1, implying that AP-1 and Ent5 are not merely components of the same carriers. We suggest that either AP-1 or Ent5 or the AP-1/Ent5 pair can recycle transmembrane TGN proteins plus an intermediate class of transmembrane Golgi proteins.

Do these two kinetic classes of transmembrane Golgi proteins actually define separate AP-1/Ent5–mediated recycling pathways? This idea has a precedent with COPI, which is a single vesicle-forming complex that mediates both Golgi-to-ER and intra-Golgi recycling (Popoff et al., 2011). Perhaps the transmembrane Golgi proteins that follow the two AP-1/Ent5–dependent pathways are not passive passengers, but are actively involved in harnessing the AP-1/Ent5 machinery to create specific types of carriers. A caveat to this interpretation is the lack of direct evidence that Golgi proteins are packaged into carriers containing AP-1 and/or Ent5. Another concern is that proteins such as Sys1 begin to depart from a maturing cisterna when the levels of membrane-associated AP-1 and Ent5 are low. This discrepancy can potentially be explained if early-arriving AP-1 and Ent5 molecules are rapidly packaged into carriers that bud from the cisternal membrane, in which case the activity of an adaptor would precede its accumulation on a cisterna. We saw such a phenomenon with a GGA-dependent vacuolar protein, which often began to depart from a maturing cisterna before a GGA adaptor showed significant accumulation (Casler and Glick, 2020). Yet another possibility is that the AP-1/Ent5 effects on proteins such as Sys1 are indirect. For example, loss of AP-1/Ent5 could inhibit a previously unknown GGA-mediated intra-Golgi recycling pathway. While these alternative explanations seem less likely, an important next step will be to characterize the AP-1/Ent5–dependent pathways in molecular terms. To this end, we are working now to determine which vesicle tethers are involved in each pathway (Wong and Munro, 2014).

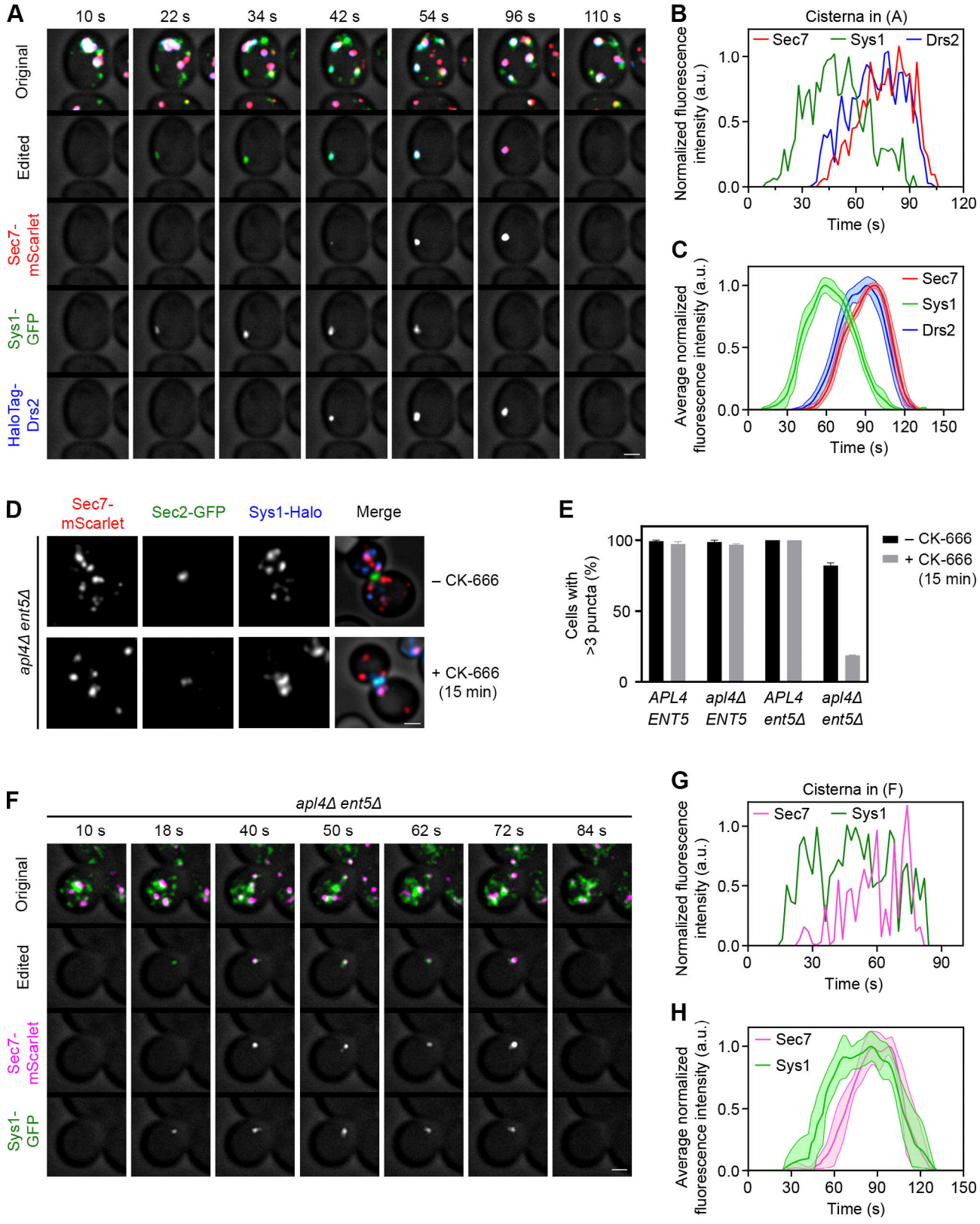

Figure 7. **Sys1 localizes with the aid of AP-1/Ent5 but has an intermediate kinetic signature. (A)** Maturation kinetics of Sys1 compared with Sec7 and Drs2. A strain expressing Sec7-mScarlet, HaloTag-Drs2, and the transmembrane Golgi protein Sys1-GFP was grown to mid-log phase, labeled with JFX dye, and imaged by 4D confocal microscopy. Shown are average projected Z-stacks at the indicated time points from part 1 of Video 7. The upper row shows the complete projections, the second row shows edited projections that include only the cisterna being tracked, and the subsequent rows show the individual fluorescence channels from the edited projections. Scale bar, 2 µm. **(B)** Quantification of tagged Golgi proteins during typical maturation events. Depicted are the normalized fluorescence intensities in arbitrary units for the cisterna tracked in A. **(C)** Smoothed and averaged traces showing the relative kinetic

signatures of Sec7, Sys1, and Drs2. Data were obtained for 10 representative cisternae. **(D)** Mislocalization of Sys1 in *apl4Δ ent5Δ* cells after CK-666 treatment. The experiment was performed as in Fig. 3 D except that Sec2-GFP was also visualized. The budded cell from the untreated culture is typical for the population, while the budded cell from the CK-666–treated culture is a striking example that illustrates the population trend. Scale bar, 2 µm. **(E)** Quantification of the effects in D. The experiment was performed as in Fig. 3 E, except that *apl4Δ ENT5* and *APL4 ent5Δ* strains were also examined. **(F)** Maturation kinetics of Sys1 compared with Sec7 in an *apl4Δ ent5Δ* strain. The experiment was performed as in A, except that HaloTag-Drs2 was not imaged because the signal was too weak. Shown are average projected Z-stacks at the indicated time points from part 2 of Video 7. Scale bar, 2 µm. **(G)** Quantification of tagged Golgi proteins during typical maturation events in an *apl4Δ ent5Δ* strain. Depicted are the normalized fluorescence intensities in arbitrary units for the cisterna tracked in F. **(H)** Smoothed and averaged traces showing the relative kinetic signatures of Sec7 and Sys1 in an *apl4Δ ent5Δ* strain. Data were obtained for seven representative cisternae. Error bars represent SEM.

A longer-term project will be to determine why the cell chooses a particular recycling pathway for a given transmembrane Golgi protein. As an example, there may be a functional explanation for why Sys1 arrives before Vps10. Sys1 initiates the recruitment of Arl1, which in turn recruits the Imh1 tether (Panic et al., 2003; Setty et al., 2003), and perhaps Imh1 then captures the carriers that recycle Vps10. This scheme fits with genetic tests of Imh1 function (Tsukada et al., 1999; Bonangelino et al., 2002; Jain et al., 2019). Answers to such questions will shed light on the mechanisms that choreograph Golgi maturation.

Golgi trafficking components tend to be highly conserved. In mammalian cells, the data are consistent with AP-1–dependent retrograde traffic at the TGN (Hinners and Tooze, 2003; Hirst et al., 2012), and many aspects of yeast Golgi protein recycling probably have counterparts in other eukaryotes. Indeed, there is evidence for several routes of intra-Golgi recycling during maturation of the mammalian Golgi (Rizzo et al., 2021). The implication is that in stacked Golgi organelles, the polarized distribution of transmembrane proteins reflects the action of multiple recycling pathways.

Materials and methods

Reagents and tools

Table S1 lists the chemicals, primers, plasmids, and software used in this study, with details about source and availability.

Yeast growth and transformation

The parental haploid *S. cerevisiae* strain was a derivative of JK9-3da (*leu2-3,112 ura3-52 rme1 trp1 his4*; Kunz et al., 1993) carrying *pdr1Δ* and *pdr3Δ* mutations to facilitate HaloTag labeling (Barrero et al., 2016). Yeast cells were grown in baffled flasks with shaking at 23°C in the nonfluorescent minimal glucose dropout medium NSD (Bevis et al., 2002) or in the rich glucose medium YPD supplemented with adenine and uracil.

Yeast proteins were tagged by gene replacement using the pop-in/pop-out method to maintain endogenous expression levels (Rothstein, 1991; Rossanese et al., 1999). Plasmid construction was simulated and recorded using SnapGene. The plasmids generated in this study have been submitted to Addgene.

Deletion of *PDR1* and *PDR3* was accomplished by replacement with a G418 or nourseothricin resistance cassette from pFA6a-kanMX6 (Bähler et al., 1998) or pAG25 (Goldstein and McCusker, 1999), respectively. Deletion of *APL4* was accomplished by using overlap extension PCR to amplify a hygromycin resistance cassette from pAG32 (Goldstein and McCusker, 1999) flanked by 500 bp upstream and downstream of the gene. Deletion of *ENT5* was accomplished using the same overlap extension PCR strategy, except that the *LEU2* gene from *Kluyveromyces lactis* was amplified from pUG73 (Gueldener et al., 2002).

CK-666 treatment

Endocytosis was inhibited by incubating cells for the indicated time periods with 100 µM CK-666 diluted from a 50-mM stock solution in DMSO. Mock treatments employed DMSO alone.

Fluorescence microscopy

Live-cell 4D confocal microscopy was performed as previously described (Johnson and Glick, 2019). Yeast strains were grown in NSD and imaged at 23°C. Cells were attached to a concanavalin A–coated coverglass-bottom dish containing NSD and were viewed on a Leica SP8 or SP5 confocal microscope equipped with a 1.4 NA/63× oil objective using a 60–80-nm pixel size, a 0.25–0.30-µm Z-step interval, and 20–30 optical sections. For time-lapse imaging, Z-stacks were captured at intervals of 2 s.

Video datasets were deconvolved with Huygens Essential software using the classic maximum likelihood estimation algorithm (Day et al., 2017). Unless otherwise indicated, static fluorescence images were also deconvolved. With the aid of ImageJ (Schneider et al., 2012), images and videos were converted to hyperstacks and average projected, then range-adjusted to maximize contrast. Previously described custom ImageJ plugins were used to generate montages of time series, select individual structures and remove extraneous signal, convert edited montages to hyperstacks, and measure fluorescence intensities (Johnson and Glick, 2019). A new custom ImageJ plugin was used to average fluorescence traces, as described below.

FM 4–64 labeling and quantification

For FM 4–64 labeling, a log-phase yeast culture was incubated for a 3–5-min pulse period with 0.8 µM FM 4–64FX diluted from a 1-mM stock in DMSO. Where indicated, external fluorescence was then quenched by addition of SCAS (4-Sulfonato calix[8] arene, sodium salt) to a final concentration of 50 µM. Fluorescence was imaged on a Leica SP8 confocal microscope.

The quantification in Fig. 1 E was performed using ImageJ. For each sample, a confocal Z-stack was average projected, and then a mask representing the TGN cisternae was created using the Sec7-GFP signal. About 10% of the TGN cisternae could not be fully resolved from FM 4–64-containing non-TGN structures such as PVE compartments, vacuoles, and sites of polarized secretion, so those TGN cisternae were manually

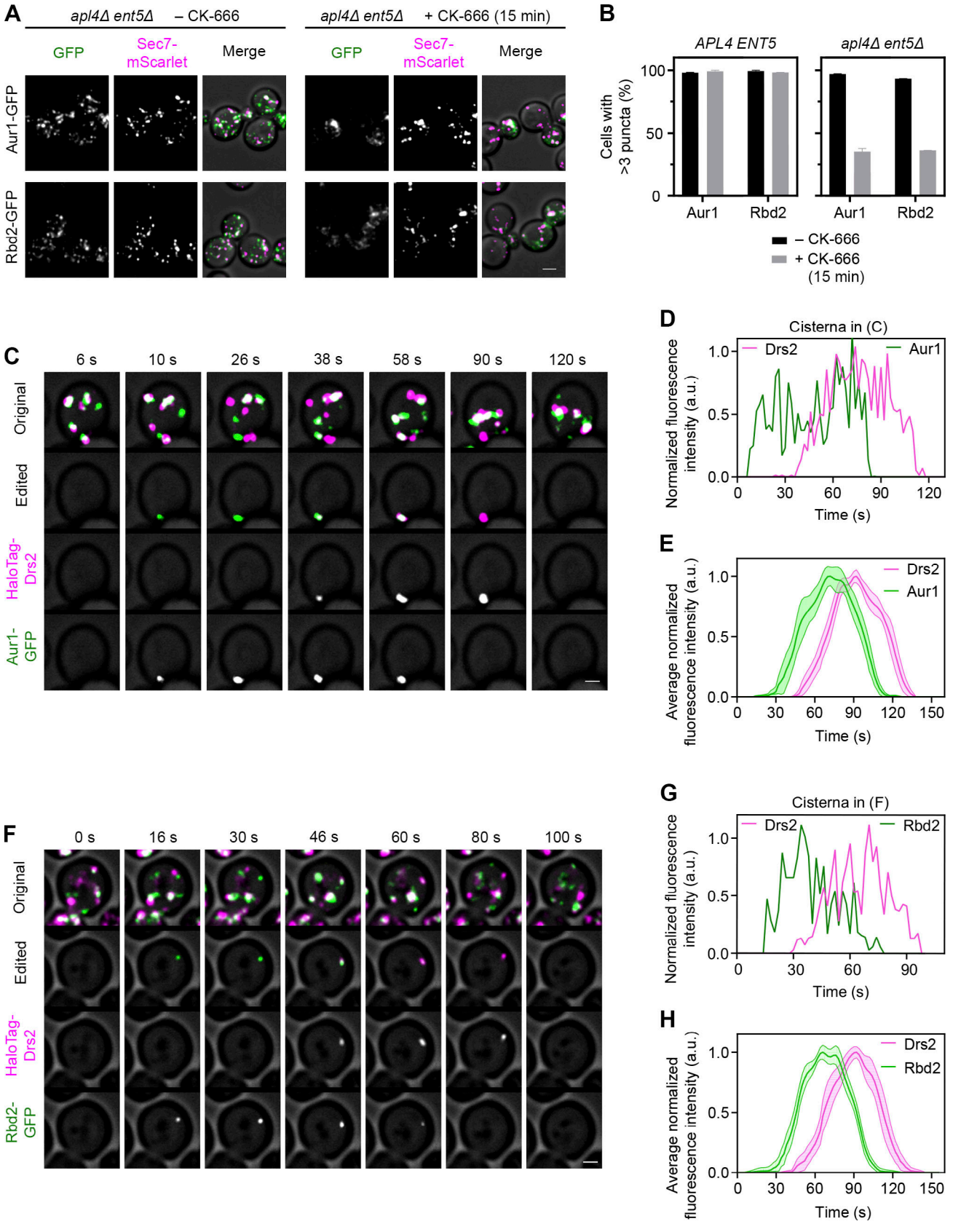

Figure 8. **Other transmembrane Golgi proteins resemble Sys1 in their kinetic signatures. (A)** Mislocalization of the transmembrane Golgi proteins Aur1 and Rbd2 in *apl4Δ ent5Δ* cells after CK-666 treatment. The experiment was performed as in Fig. 3 D. Scale bar, 2 µm. **(B)** Quantification of the effects in A. The experiment was performed as in Fig. 3 E. **(C)** Maturation kinetics of Drs2 compared with Aur1. A strain expressing HaloTag-Drs2 and Aur1-GFP was grown to

mid-log phase, labeled with JFX dye, and imaged by 4D confocal microscopy. Shown are average projected Z-stacks at the indicated time points from part 1 of Video 8. The upper row shows the complete projections, the second row shows edited projections that include only the cisterna being tracked, and the subsequent rows show the individual fluorescence channels from the edited projections. Scale bar, 2 µm. **(D)** Quantification of tagged Golgi proteins during typical maturation events. Depicted are the normalized fluorescence intensities in arbitrary units for the cisterna tracked in C. **(E)** Smoothed and averaged traces showing the relative kinetic signatures of Drs2 and Aur1. Data were obtained for 10 representative cisternae. **(F)** Maturation kinetics of Drs2 compared with Rbd2. The experiment was performed as in C, except with a strain expressing HaloTag-Drs2 and Rbd2-GFP. Shown are average projected Z-stacks at the indicated time points from part 2 of Video 8. Scale bar, 2 µm. **(G)** Quantification of tagged Golgi proteins during typical maturation events. Depicted are the normalized fluorescence intensities in arbitrary units for the cisterna tracked in F. **(H)** Smoothed and averaged traces showing the relative kinetic signatures of Drs2 and Rbd2. Data were obtained for 14 representative cisternae. Error bars represent SEM.

removed from the mask. The FM 4–64 signal within the adjusted mask was quantified for each cell, and this value was corrected by subtracting a background signal obtained from cell-free areas of the image.

HaloTag labeling

HaloTag labeling was performed as previously described (Casler et al., 2019). To visualize proteins fused to HaloTag, JFX_{646} or JFX_{650} ligand (Grimm et al., 2021), kindly provided by Luke Lavis (Janelia Research Campus, Ashburn, VA), was diluted 1:1,000 from a 1-mM stock in DMSO in 0.5 ml of culture medium to give a final concentration of 1 µM. The medium was cleared of any precipitate by spinning at 17,000×*g* (13,000 rpm) in a microcentrifuge for 1 min. Then the cleared medium containing ligand was added to 0.5 ml of log-phase yeast culture, and the cells were incubated with shaking at 23°C for 30 min. Excess dye was removed by filtration through and washing on a 0.22-µm syringe filter (Millipore; catalog #SLGV004SL). The washed cells were resuspended in NSD and attached to a concanavalin A–coated coverglass-bottom dish. Videos were captured immediately by confocal microscopy.

Statistical analysis

Calculation and plotting of mean and SEM values were performed using Prism software. Each figure legend indicates the number of data points and experimental replicates.

Quantification and averaging of Golgi maturation events

Two- and three-color 4D confocal microscopy traces of individual cisternae containing tagged Golgi proteins were analyzed and quantified using custom ImageJ plugins as previously described (Johnson and Glick, 2019). For a single cisterna, the fluorescence trace in each channel was normalized to the average of the three highest values. For smoothing and averaging, a new custom ImageJ plugin was written to perform the following operations.

The first step was to smooth each noisy trace. For this purpose, a trace was numerically integrated, and then the integral was numerically differentiated using the smoothing method of Pavel Holoborodko (Holoborodko, 2021) with $n = 2$, $n = 11$. The numerical differentiation formula is as follows. If f_0 represents a given point in the integral, and f_1 represents the next point, and f_{-1} represents the previous point, and so on, then the derivative at the point is estimated as

$$\begin{bmatrix} 42(f_1 - f_{-1}) + 48(f_2 - f_{-2}) + \\ 27(f_3 - f_{-3}) + 8(f_4 - f_{-4}) + f_5 - f_{-5} \end{bmatrix} \Big/ 512$$

The peak of a smoothed trace was defined as the 50% point of the integral. To estimate the start and end points of a smoothed trace, a line was defined by the two time points when the trace first rose above 10% of its maximum value, and a second line was defined by the two time points when the trace permanently sank below 10% of its maximum value, and then these lines were extrapolated to the horizontal (time) axis.

The next step was to average the smoothed traces. For a given fluorescence channel, each smoothed trace was normalized to a maximum value of 1.0, and then the smoothed traces were averaged by centering at the peak values. The averaged trace was normalized to a maximum value of 1.0. To show multiple fluorescence channels on the same plot, the offset between any two fluorescence channels was calculated by measuring for each individual cisterna the offset between the peak values for the smoothed traces in the two channels and then averaging those offset values. Plots of averaged traces show solid lines for mean values plus shaded areas for 95% confidence intervals calculated by determining the SEM at each point and multiplying by 1.96. Relative arrival and departure times for two tagged Golgi proteins were calculated by measuring for each individual cisterna the offsets in start and end points for the smoothed traces in the two fluorescence channels and then averaging those offset values.

The ImageJ plugins used for this study are available from a GitHub repository: https://github.com/bsglicker/4D-Image-Analysis.

Online supplemental material

Fig. S1 and Fig. S2 show the effects of CK-666 on transmembrane TGN proteins in wild-type cells (Fig. S1) or in cells lacking either AP-1 or Ent5 (Fig. S2). Fig. S3 shows a quantification of the CK-666 effects on transmembrane Golgi proteins in cells lacking both AP-1 and Ent5. Fig. S4 and Fig. S5 show the kinetic signatures of various TGN proteins (Fig. S4) and early Golgi proteins (Fig. S5). Video 1, Video 2, Video 3, Video 4, Video 5, Video 6, Video 7, and Video 8 show the original 4D confocal data for the maturing Golgi cisternae analyzed in the figures. Table S1 lists the reagents and tools used in this study.

Acknowledgments

Jasper Jeffrey contributed to construction of the YIplac211-ANP1-msGFP2 plasmid. Thanks for assistance with fluorescence microscopy to Vytas Bindokas and Christine Labno at the Integrated Microscopy Core Facility, which is supported by the National Institutes of Health (NIH)–funded Cancer Center Support Grant

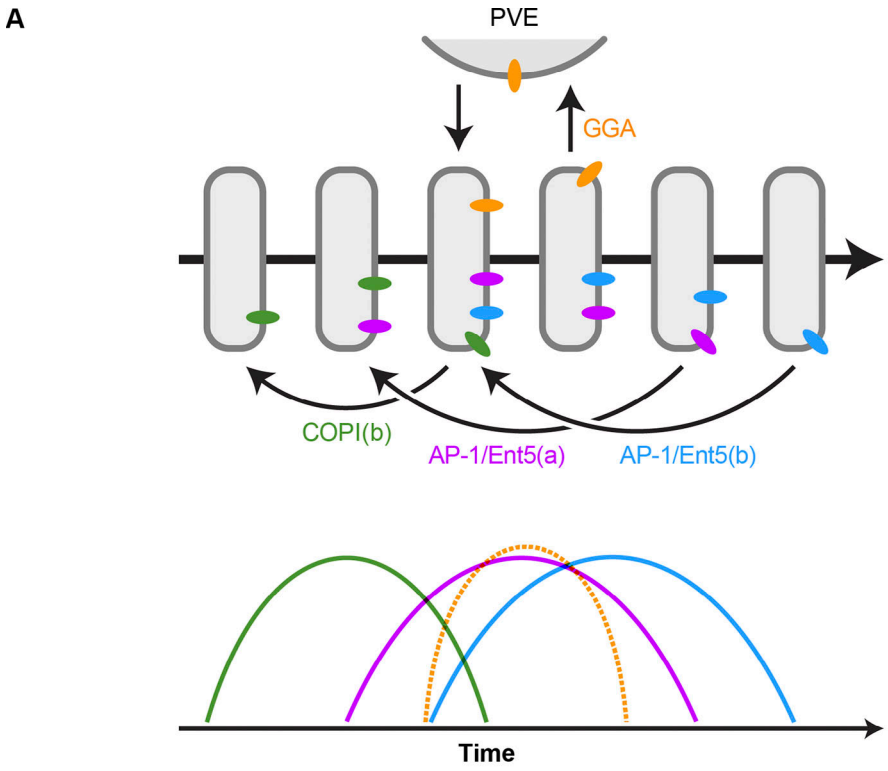

B

Golgi Protein	Inferred Recycling Pathway	Arrival Relative to Drs2 (s)	Departure Relative to Drs2 (s)
Vrg4	COPI(b)	-53.9 ± 5.5	-57.0 ± 3.7
Anp1	COPI(b)	-54.0 ± 5.7	-60.0 ± 6.4
Mnn9	COPI(b)	-69.0 ± 6.0	-59.9 ± 6.2
Sys1	AP-1/Ent5(a)	-20.6 ± 3.1	-15.4 ± 2.3
Aur1	AP-1/Ent5(a)	-17.2 ± 1.8	-19.3 ± 3.2
Rbd2	AP-1/Ent5(a)	-19.1 ± 2.1	-18.6 ± 1.5
Vps10	GGAs + PVE-to-Golgi	-6.5 ± 0.9	-25.9 ± 2.1
Nhx1	GGAs + PVE-to-Golgi	-1.6 ± 2.0	-23.1 ± 2.8
Drs2	AP-1/Ent5(b)	– –	– –
Tlg1	AP-1/Ent5(b)	-0.3 ± 1.0	-6.4 ± 0.6*
Kex2	AP-1/Ent5(b)	-2.6 ± 1.2	-9.9 ± 2.0*
Ste13	AP-1/Ent5(b)	-2.5 ± 1.1	-15.5 ± 2.5*
Stv1	AP-1/Ent5(b)	-1.6 ± 0.7	-11.1 ± 1.6*

* For unknown reasons, Drs2 departed somewhat later than the other TGN proteins that were examined.

Figure 9. **Recycling pathways determine the kinetic signatures and localizations of transmembrane Golgi proteins. (A)** Model of Golgi recycling pathways and corresponding kinetic signatures. Straight horizontal arrows represent time during the life cycle of a cisterna, other arrows represent traffic pathways, rounded rectangles represent Golgi cisternae of different ages, and colored ovals represent transmembrane proteins. Based on evidence presented here and elsewhere, we suggest that there are three sequential intra-Golgi recycling pathways. The first pathway is designated COPI(b) to distinguish it from COPI(a)-mediated Golgi-to-ER recycling, which is not depicted. This COPI(b) pathway generates early kinetic signatures (green). The second pathway is designated AP-1/Ent5(a), and it recycles proteins such as Sys1 to generate intermediate kinetic signatures (magenta). The third pathway is designated AP-1/Ent5(b), and it recycles TGN proteins such as Drs2 to generate late kinetic signatures (blue). In addition, a pathway of GGA-dependent transport to PVE compartments followed by recycling to nascent TGN cisternae generates separate kinetic signatures (orange). For a given transmembrane Golgi protein, the kinetic signature governs localization to cisternae in a particular age range. Some Golgi proteins might follow more than one pathway, in which case their kinetic signatures would be combinations of the ones depicted here. **(B)** Quantification of kinetic signatures for Golgi transmembrane proteins that are believed to follow four distinct recycling pathways. The colors match those in A. Shown are average and SEM values for arrival and departure times relative to Drs2, based on the same data that were used to generate plots in other figures. Negative numbers indicate arrival or departure earlier than Drs2. The average signal duration for Drs2 was 68.8 ± 1.2 s based on a total of 157 traces, with nearly all of the events in the range of 40–90 s.

P30 CA014599. We thank Luke Lavis for providing the JFX_{646} and JFX_{650} dyes.

This work in the B.S. Glick laboratory was supported by NIH grant R01 GM137004. J.C. Casler, A.H. Krahn, and K.J. Day were supported by NIH training grant T32 GM007183.

The authors declare no competing financial interests.

Author contributions: Conceptualization, J.C. Casler and B.S. Glick; Methodology, J.C. Casler and B.S. Glick; Software, B.S. Glick; Investigation, J.C. Casler, N. Johnson, A.H. Krahn, and A. Pantazopoulou; Resources, J.C. Casler, N. Johnson, A.H. Krahn, A. Pantazopoulou, and K.J. Day; Writing—Original Draft, J.C. Casler and B.S. Glick; Writing—Review and Editing, J.C. Casler and B.S. Glick; Visualization, J.C. Casler and N. Johnson; Supervision, B.S. Glick; and Funding Acquisition, B.S. Glick.

Submitted: 29 March 2021
Revised: 16 September 2021
Accepted: 26 October 2021

References

Abe, M., Y. Noda, H. Adachi, and K. Yoda. 2004. Localization of GDP-mannose transporter in the Golgi requires retrieval to the endoplasmic reticulum depending on its cytoplasmic tail and coatomer. *J. Cell Sci.* 117: 5687–5696. https://doi.org/10.1242/jcs.01491

Antkowiak, A., A. Guillotin, M.B. Sanders, J. Colombo, R. Vincentelli, and A. Michelot. 2019. Sizes of actin networks sharing a common environment are determined by the relative rates of assembly. *PLoS Biol.* 17:e3000317. https://doi.org/10.1371/journal.pbio.3000317

Bähler, J., J.Q. Wu, M.S. Longtine, N.G. Shah, A. McKenzie III, A.B. Steever, A. Wach, P. Philippsen, and J.R. Pringle. 1998. Heterologous modules for efficient and versatile PCR-based gene targeting in *Schizosaccharomyces pombe*. *Yeast.* 14:943–951. https://doi.org/10.1002/(SICI)1097-0061(199807)14:10<943::AID-YEA292>3.0.CO;2-Y

Banfield, D.K. 2011. Mechanisms of protein retention in the Golgi. *Cold Spring Harb. Perspect. Biol.* 3:a005264. https://doi.org/10.1101/cshperspect.a005264

Barlowe, C.K., and E.A. Miller. 2013. Secretory protein biogenesis and traffic in the early secretory pathway. *Genetics.* 193:383–410. https://doi.org/10.1534/genetics.112.142810

Barrero, J.J., E. Papanikou, J.C. Casler, K.J. Day, and B.S. Glick. 2016. An improved reversibly dimerizing mutant of the FK506-binding protein FKBP. *Cell. Logist.* 6:e1204848. https://doi.org/10.1080/21592799.2016.1204848

Behnia, R., B. Panic, J.R. Whyte, and S. Munro. 2004. Targeting of the Arf-like GTPase Arl3p to the Golgi requires N-terminal acetylation and the membrane protein Sys1p. *Nat. Cell Biol.* 6:405–413. https://doi.org/10.1038/ncb1120

Bevis, B.J., A.T. Hammond, C.A. Reinke, and B.S. Glick. 2002. *De novo* formation of transitional ER sites and Golgi structures in *Pichia pastoris*. *Nat. Cell Biol.* 4:750–756. https://doi.org/10.1038/ncb852

Black, M.W., and H.R. Pelham. 2000. A selective transport route from Golgi to late endosomes that requires the yeast GGA proteins. *J. Cell Biol.* 151: 587–600. https://doi.org/10.1083/jcb.151.3.587

Bonangelino, C.J., E.M. Chavez, and J.S. Bonifacino. 2002. Genomic screen for vacuolar protein sorting genes in *Saccharomyces cerevisiae*. *Mol. Biol. Cell.* 13:2486–2501. https://doi.org/10.1091/mbc.02-01-0005

Bryant, N.J., and T.H. Stevens. 1997. Two separate signals act independently to localize a yeast late Golgi membrane protein through a combination of retrieval and retention. *J. Cell Biol.* 136:287–297. https://doi.org/10.1083/jcb.136.2.287

Burke, T.A., J.R. Christensen, E. Barone, C. Suarez, V. Sirotkin, and D.R. Kovar. 2014. Homeostatic actin cytoskeleton networks are regulated by assembly factor competition for monomers. *Curr. Biol.* 24:579–585. https://doi.org/10.1016/j.cub.2014.01.072

Casler, J.C., and B.S. Glick. 2019. Visualizing secretory cargo transport in budding yeast. *Curr. Protoc. Cell Biol.* 83:e80. https://doi.org/10.1002/cpcb.80

Casler, J.C., and B.S. Glick. 2020. A microscopy-based kinetic analysis of yeast vacuolar protein sorting. *eLife.* 9:e56844. https://doi.org/10.7554/eLife.56844

Casler, J.C., E. Papanikou, J.J. Barrero, and B.S. Glick. 2019. Maturation-driven transport and AP-1-dependent recycling of a secretory cargo in the Golgi. *J. Cell Biol.* 218:1582–1601. https://doi.org/10.1083/jcb.201807195

Chi, R.J., J. Liu, M. West, J. Wang, G. Odorizzi, and C.G. Burd. 2014. Fission of SNX-BAR-coated endosomal retrograde transport carriers is promoted by the dynamin-related protein Vps1. *J. Cell Biol.* 204:793–806. https://doi.org/10.1083/jcb.201309084

Conibear, E., and T.H. Stevens. 1998. Multiple sorting pathways between the late Golgi and the vacuole in yeast. *Biochim. Biophys. Acta.* 1404:211–230. https://doi.org/10.1016/S0167-4889(98)00058-5

Cooper, A.A., and T.H. Stevens. 1996. Vps10p cycles between the late-Golgi and prevacuolar compartments in its function as the sorting receptor for multiple yeast vacuolar hydrolases. *J. Cell Biol.* 133:529–541. https://doi.org/10.1083/jcb.133.3.529

Čopič, A., T.L. Starr, and R. Schekman. 2007. Ent3p and Ent5p exhibit cargo-specific functions in trafficking proteins between the *trans*-Golgi network and the endosomes in yeast. *Mol. Biol. Cell.* 18:1803–1815. https://doi.org/10.1091/mbc.e06-11-1000

Cortesio, C.L., E.B. Lewellyn, and D.G. Drubin. 2015. Control of lipid organization and actin assembly during clathrin-mediated endocytosis by the cytoplasmic tail of the rhomboid protein Rbd2. *Mol. Biol. Cell.* 26: 1509–1522. https://doi.org/10.1091/mbc.E14-11-1540

Costaguta, G., M.C. Duncan, G.E. Fernández, G.H. Huang, and G.S. Payne. 2006. Distinct roles for TGN/endosome epsin-like adaptors Ent3p and Ent5p. *Mol. Biol. Cell.* 17:3907–3920. https://doi.org/10.1091/mbc.e06-05-0410

Daboussi, L., G. Costaguta, and G.S. Payne. 2012. Phosphoinositide-mediated clathrin adaptor progression at the *trans*-Golgi network. *Nat. Cell Biol.* 14:239–248. https://doi.org/10.1038/ncb2427

Day, K.J., P.J. La Rivière, T. Chandler, V.P. Bindokas, N.J. Ferrier, and B.S. Glick. 2017. Improved deconvolution of very weak confocal signals. *F1000Res.* 6:787. https://doi.org/10.12688/f1000research.11773.1

Day, K.J., J.C. Casler, and B.S. Glick. 2018. Budding yeast has a minimal endomembrane system. *Dev. Cell.* 44:56–72.E4. https://doi.org/10.1016/j.devcel.2017.12.014

De Matteis, M.A., and A. Luini. 2008. Exiting the Golgi complex. *Nat. Rev. Mol. Cell Biol.* 9:273–284. https://doi.org/10.1038/nrm2378

Dell'Angelica, E.C., R. Puertollano, C. Mullins, R.C. Aguilar, J.D. Vargas, L.M. Hartnell, and J.S. Bonifacino. 2000. Ggas: a family of ADP ribosylation factor-binding proteins related to adaptors and associated with the Golgi complex. *J. Cell Biol.* 149:81–94. https://doi.org/10.1083/jcb.149.1.81

Deng, Y., Y. Guo, H. Watson, W.C. Au, M. Shakoury-Elizeh, M.A. Basrai, J.S. Bonifacino, and C.C. Philpott. 2009. Gga2 mediates sequential ubiquitin-independent and ubiquitin-dependent steps in the trafficking of ARN1 from the *trans*-Golgi network to the vacuole. *J. Biol. Chem.* 284:23830–23841. https://doi.org/10.1074/jbc.M109.030015

Duncan, M.C., G. Costaguta, and G.S. Payne. 2003. Yeast epsin-related proteins required for Golgi-endosome traffic define a gamma-adaptin ear-binding motif. *Nat. Cell Biol.* 5:77–81. https://doi.org/10.1038/ncb901

Dunphy, W.G., and J.E. Rothman. 1985. Compartmental organization of the Golgi stack. *Cell.* 42:13–21. https://doi.org/10.1016/S0092-8674(85)80097-0

Elkind, N.B., C. Walch-Solimena, and P.J. Novick. 2000. The role of the COOH terminus of Sec2p in the transport of post-Golgi vesicles. *J. Cell Biol.* 149: 95–110. https://doi.org/10.1083/jcb.149.1.95

Farquhar, M.G., and G.E. Palade. 1981. The Golgi apparatus (complex) - (1954-1981) - from artifact to center stage. *J. Cell Biol.* 91:77s–103s. https://doi.org/10.1083/jcb.91.3.77s

Finger, F.P., and P. Novick. 1998. Spatial regulation of exocytosis: lessons from yeast. *J. Cell Biol.* 142:609–612. https://doi.org/10.1083/jcb.142.3.609

Finnigan, G.C., G.E. Cronan, H.J. Park, S. Srinivasan, F.A. Quiocho, and T.H. Stevens. 2012. Sorting of the yeast vacuolar-type, proton-translocating ATPase enzyme complex (V-ATPase): identification of a necessary and sufficient Golgi/endosomal retention signal in Stv1p. *J. Biol. Chem.* 287: 19487–19500. https://doi.org/10.1074/jbc.M112.343814

Foote, C., and S.F. Nothwehr. 2006. The clathrin adaptor complex 1 directly binds to a sorting signal in Ste13p to reduce the rate of its trafficking to the late endosome of yeast. *J. Cell Biol.* 173:615–626. https://doi.org/10.1083/jcb.200510161

Fuller, R.S., R.E. Sterne, and J. Thorner. 1988. Enzymes required for yeast prohormone processing. *Annu. Rev. Physiol.* 50:345–362. https://doi.org/10.1146/annurev.ph.50.030188.002021

Gaynor, E.C., T.R. Graham, and S.D. Emr. 1998. COPI in ER/Golgi and intra-Golgi transport: do yeast COPI mutants point the way? *Biochim. Biophys. Acta.* 1404:33–51. https://doi.org/10.1016/S0167-4889(98)00045-7

Gillingham, A.K., and S. Munro. 2016. Finding the Golgi: golgin coiled-coil proteins show the way. *Trends Cell Biol.* 26:399–408. https://doi.org/10.1016/j.tcb.2016.02.005

Glick, B.S., and A. Luini. 2011. Models for Golgi traffic: a critical assessment. *Cold Spring Harb. Perspect. Biol.* 3:a005215. https://doi.org/10.1101/cshperspect.a005215

Glick, B.S., and A. Nakano. 2009. Membrane traffic within the Golgi stack. *Annu. Rev. Cell Dev. Biol.* 25:113–132. https://doi.org/10.1146/annurev.cellbio.24.110707.175421

Glick, B.S., T. Elston, and G. Oster. 1997. A cisternal maturation mechanism can explain the asymmetry of the Golgi stack. *FEBS Lett.* 414:177–181. https://doi.org/10.1016/S0014-5793(97)00984-8

Goldstein, A.L., and J.H. McCusker. 1999. Three new dominant drug resistance cassettes for gene disruption in *Saccharomyces cerevisiae*. *Yeast.* 15:1541–1553. https://doi.org/10.1002/(SICI)1097-0061(199910)15:14<1541::AID-YEA476>3.0.CO;2-K

Goode, B.L., A.A. Rodal, G. Barnes, and D.G. Drubin. 2001. Activation of the Arp2/3 complex by the actin filament binding protein Abp1p. *J. Cell Biol.* 153:627–634. https://doi.org/10.1083/jcb.153.3.627

Grimm, J.B., L. Xie, J.C. Casler, R. Patel, A.N. Tkachuk, N. Falco, H. Choi, J. Lippincott-Schwartz, T.A. Brown, B.S. Glick, et al. 2021. A general method to improve fluorophores using deterated auxochromes. *JACS Au.* 1:690–696. https://doi.org/10.1021/jacsau.1c00006

Gueldener, U., J. Heinisch, G.J. Koehler, D. Voss, and J.H. Hegemann. 2002. A second set of *loxP* marker cassettes for Cre-mediated multiple gene knockouts in budding yeast. *Nucleic Acids Res.* 30:e23. https://doi.org/10.1093/nar/30.6.e23

Harrison, M.S., C.S. Hung, T. Liu, R. Christiano, T.C. Walther, and C.G. Burd. 2014. A mechanism for retromer endosomal coat complex assembly with cargo. *Proc. Natl. Acad. Sci. USA.* 111:267–272. https://doi.org/10.1073/pnas.1316482111

Hetrick, B., M.S. Han, L.A. Helgeson, and B.J. Nolen. 2013. Small molecules CK-666 and CK-869 inhibit actin-related protein 2/3 complex by blocking an activating conformational change. *Chem. Biol.* 20:701–712. https://doi.org/10.1016/j.chembiol.2013.03.019

Hinners, I., and S.A. Tooze. 2003. Changing directions: clathrin-mediated transport between the Golgi and endosomes. *J. Cell Sci.* 116:763–771. https://doi.org/10.1242/jcs.00270

Hirst, J., W.W.Y. Lui, N.A. Bright, N. Totty, M.N.J. Seaman, and M.S. Robinson. 2000. A family of proteins with γ-adaptin and VHS domains that facilitate trafficking between the TGN and the vacuole/lysosome. *J. Cell Biol.* 149:67–80. https://doi.org/10.1083/jcb.149.1.67

Hirst, J., G.H. Borner, R. Antrobus, A.A. Peden, N.A. Hodson, D.A. Sahlender, and M.S. Robinson. 2012. Distinct and overlapping roles for AP-1 and GGAs revealed by the "knocksideways" system. *Curr. Biol.* 22:1711–1716. https://doi.org/10.1016/j.cub.2012.07.012

Holoborodko, P. 2021. Smooth noise-robust differentiators. http://www.holoborodko.com/pavel/numerical-methods/numerical-derivative/smooth-low-noise-differentiators/ (accessed November 2, 2021).

Huckaba, T.M., A.C. Gay, L.F. Pantalena, H.C. Yang, and L.A. Pon. 2004. Live cell imaging of the assembly, disassembly, and actin cable-dependent movement of endosomes and actin patches in the budding yeast, *Saccharomyces cerevisiae*. *J. Cell Biol.* 167:519–530. https://doi.org/10.1083/jcb.200404173

Hung, C.W., and M.C. Duncan. 2016. Clathrin binding by the adaptor Ent5 promotes late stages of clathrin coat maturation. *Mol. Biol. Cell.* 27:1143–1153. https://doi.org/10.1091/mbc.E15-08-0588

Ishii, M., Y. Suda, H. Kurokawa, and A. Nakano. 2016. COPI is essential for Golgi cisternal maturation and dynamics. *J. Cell Sci.* 129:3251–3261. https://doi.org/10.1242/jcs.193367

Jain, B.K., R. Dahara, and D. Bhattacharyya. 2019. The golgin *Pp*Imh1 mediates reversible cisternal stacking in the Golgi of the budding yeast *Pichia pastoris*. *J. Cell Sci.* 132:jcs230672. https://doi.org/10.1242/jcs.230672

Johansen, J., G. Alfaro, and C.T. Beh. 2016. Polarized exocytosis induces compensatory endocytosis by Sec4p-regulated cortical actin polymerization. *PLoS Biol.* 14:e1002534. https://doi.org/10.1371/journal.pbio.1002534

Johnson, N., and B.S. Glick. 2019. 4D microscopy of yeast. *J. Vis. Exp.* (146). https://doi.org/10.3791/58618

Jungmann, J., and S. Munro. 1998. Multi-protein complexes in the *cis* Golgi of *Saccharomyces cerevisiae* with α-1,6-mannosyltransferase activity. *EMBO J.* 17:423–434. https://doi.org/10.1093/emboj/17.2.423

Kim, J.J., Z. Lipatova, and N. Segev. 2016. Regulation of Golgi cisternal progression by Ypt/Rab GTPases. *Dev. Cell.* 36:440–452. https://doi.org/10.1016/j.devcel.2016.01.016

Kojima, A., J.Y. Toshima, C. Kanno, C. Kawata, and J. Toshima. 2012. Localization and functional requirement of yeast Na+/H+ exchanger, Nhx1p, in the endocytic and protein recycling pathway. *Biochim. Biophys. Acta.* 1823:534–543. https://doi.org/10.1016/j.bbamcr.2011.12.004

Kunz, J., U. Schneider, M. Deuter-Reinhard, N.R. Movva, and M.N. Hall. 1993. Target of rapamycin in yeast, TOR2, is an essential phosphatidylinositol kinase homolog required for G1 progression. *Cell.* 73:585–596. https://doi.org/10.1016/0092-8674(93)90144-F

Kurokawa, K., O. Osakada, T. Kodijani, M. Waga, Y. Suda, H. Asakawa, T. Haraguchi, and A. Nakano. 2019. Visualization of secretory cargo transport within the Golgi apparatus. *J. Cell Biol.* 218:1602–1618. https://doi.org/10.1083/jcb.201807194

Lastun, V.L., A.G. Grieve, and M. Freeman. 2016. Substrates and physiological functions of secretase rhomboid proteases. *Semin. Cell Dev. Biol.* 60:10–18. https://doi.org/10.1016/j.semcdb.2016.07.033

Levine, T.P., C.A. Wiggins, and S. Munro. 2000. Inositol phosphorylceramide synthase is located in the Golgi apparatus of *Saccharomyces cerevisiae*. *Mol. Biol. Cell.* 11:2267–2281. https://doi.org/10.1091/mbc.11.7.2267

Lewis, M.J., B.J. Nichols, C. Prescianotto-Baschong, H. Riezman, and H.R.B. Pelham. 2000. Specific retrieval of the exocytic SNARE Snc1p from early yeast endosomes. *Mol. Biol. Cell.* 11:23–38. https://doi.org/10.1091/mbc.11.1.23

Liu, K., K. Surendhran, S.F. Nothwehr, and T.R. Graham. 2008. P4-ATPase requirement for AP-1/clathrin function in protein transport from the *trans*-Golgi network and early endosomes. *Mol. Biol. Cell.* 19:3526–3535. https://doi.org/10.1091/mbc.e08-01-0025

Losev, E., C.A. Reinke, J. Jellen, D.E. Strongin, B.J. Bevis, and B.S. Glick. 2006. Golgi maturation visualized in living yeast. *Nature.* 441:1002–1006. https://doi.org/10.1038/nature04717

Ma, M., and C.G. Burd. 2020. Retrograde trafficking and plasma membrane recycling pathways of the budding yeast *Saccharomyces cerevisiae*. *Traffic.* 21:45–59. https://doi.org/10.1111/tra.12693

Manolson, M.F., B. Wu, D. Proteau, B.E. Taillon, B.T. Roberts, M.A. Hoyt, and E.W. Jones. 1994. *STV1* gene encodes functional homologue of 95-kDa yeast vacuolar H(+)-ATPase subunit Vph1p. *J. Biol. Chem.* 269:14064–14074. https://doi.org/10.1016/S0021-9258(17)36755-8

Marcusson, E.G., B.F. Horazdovsky, J. Lin Cereghino, E. Gharakhanian, and S.D. Emr. 1994. The sorting receptor for yeast vacuolar carboxypeptidase Y is encoded by the *VPS10* gene. *Cell.* 77:579–586. https://doi.org/10.1016/0092-8674(94)90219-4

Mellman, I., and K. Simons. 1992. The Golgi complex: in vitro veritas? *Cell.* 68:829–840. https://doi.org/10.1016/0092-8674(92)90027-A

Mizuno-Yamasaki, E., M. Medkova, J. Coleman, and P. Novick. 2010. Phosphatidylinositol 4-phosphate controls both membrane recruitment and a regulatory switch of the Rab GEF Sec2p. *Dev. Cell.* 18:828–840. https://doi.org/10.1016/j.devcel.2010.03.016

Mowbrey, K., and J.B. Dacks. 2009. Evolution and diversity of the Golgi body. *FEBS Lett.* 583:3738–3745. https://doi.org/10.1016/j.febslet.2009.10.025

Munro, S. 2002. Organelle identity and the targeting of peripheral membrane proteins. *Curr. Opin. Cell Biol.* 14:506–514. https://doi.org/10.1016/S0955-0674(02)00350-2

Myers, M.D., and G.S. Payne. 2013. Clathrin, adaptors and disease: insights from the yeast *Saccharomyces cerevisiae*. *Front. Biosci. (Landmark Ed).* 18:862–891. https://doi.org/10.2741/4149

Nagiec, M.M., E.E. Nagiec, J.A. Baltisberger, G.B. Wells, R.L. Lester, and R.C. Dickson. 1997. Sphingolipid synthesis as a target for antifungal drugs. Complementation of the inositol phosphorylceramide synthase defect in a mutant strain of *Saccharomyces cerevisiae* by the *AUR1* gene. *J. Biol. Chem.* 272:9809–9817. https://doi.org/10.1074/jbc.272.15.9809

Nothwehr, S.F., S.A. Ha, and P. Bruinsma. 2000. Sorting of yeast membrane proteins into an endosome-to-Golgi pathway involves direct interaction of their cytosolic domains with Vps35p. *J. Cell Biol.* 151:297–310. https://doi.org/10.1083/jcb.151.2.297

Panic, B., J.R. Whyte, and S. Munro. 2003. The ARF-like GTPases Arl1p and Arl3p act in a pathway that interacts with vesicle-tethering factors at the Golgi apparatus. *Curr. Biol.* 13:405–410. https://doi.org/10.1016/S0960-9822(03)00091-5

Pantazopoulou, A., and B.S. Glick. 2019. A kinetic view of membrane traffic pathways can transcend the classical view of Golgi compartments. *Front. Cell Dev. Biol.* 7:153. https://doi.org/10.3389/fcell.2019.00153

Papanikou, E., and B.S. Glick. 2009. The yeast Golgi apparatus: insights and mysteries. *FEBS Lett.* 583:3746–3751. https://doi.org/10.1016/j.febslet.2009.10.072

Papanikou, E., K.J. Day, J. Austin II, and B.S. Glick. 2015. COPI selectively drives maturation of the early Golgi. *eLife.* 4:e13232. https://doi.org/10.7554/eLife.13232

Patterson, G.H., K. Hirschberg, R.S. Polishchuk, D. Gerlich, R.D. Phair, and J. Lippincott-Schwartz. 2008. Transport through the Golgi apparatus by

rapid partitioning within a two-phase membrane system. *Cell.* 133: 1055–1067. https://doi.org/10.1016/j.cell.2008.04.044

Pellett, P.A., F. Dietrich, J. Bewersdorf, J.E. Rothman, and G. Lavieu. 2013. Inter-Golgi transport mediated by COPI-containing vesicles carrying small cargoes. *eLife.* 2:e01296. https://doi.org/10.7554/eLife.01296

Pfeffer, S.R. 2010. How the Golgi works: a cisternal progenitor model. *Proc. Natl. Acad. Sci. USA.* 107:19614–19618. https://doi.org/10.1073/pnas.1011016107

Popoff, V., F. Adolf, B. Brügger, and F. Wieland. 2011. COPI budding within the Golgi stack. *Cold Spring Harb. Perspect. Biol.* 3:a005231. https://doi.org/10.1101/cshperspect.a005231

Rabouille, C., and J. Klumperman. 2005. The maturing role of COPI vesicles in intra-Golgi transport. *Nat. Rev. Mol. Cell Biol.* 6:812–817. https://doi.org/10.1038/nrm1735

Rabouille, C., N. Hui, F. Hunte, R. Kieckbusch, E.G. Berger, G. Warren, and T. Nilsson. 1995. Mapping the distribution of Golgi enzymes involved in the construction of complex oligosaccharides. *J. Cell Sci.* 108:1617–1627. https://doi.org/10.1242/jcs.108.4.1617

Riezman, H. 1985. Endocytosis in yeast: several of the yeast secretory mutants are defective in endocytosis. *Cell.* 40:1001–1009. https://doi.org/10.1016/0092-8674(85)90360-5

Rizzo, R., D. Russo, K. Kurokawa, P. Sahu, B. Lombardi, D. Supino, M.A. Zhukovsky, A. Vocat, P. Pothukuchi, V. Kunnathully, et al. 2021. Golgi maturation-dependent glycoenzyme recycling controls glycosphingolipid biosynthesis and cell growth via GOLPH3. *EMBO J.* 40:e107238. https://doi.org/10.15252/embj.2020107238

Rossanese, O.W., J. Soderholm, B.J. Bevis, I.B. Sears, J. O'Connor, E.K. Williamson, and B.S. Glick. 1999. Golgi structure correlates with transitional endoplasmic reticulum organization in *Pichia pastoris* and *Saccharomyces cerevisiae*. *J. Cell Biol.* 145:69–81. https://doi.org/10.1083/jcb.145.1.69

Rothstein, R. 1991. Targeting, disruption, replacement, and allele rescue: integrative DNA transformation in yeast. *Methods Enzymol.* 194:281–301. https://doi.org/10.1016/0076-6879(91)94022-5

Schneider, C.A., W.S. Rasband, and K.W. Eliceiri. 2012. NIH Image to ImageJ: 25 years of image analysis. *Nat. Methods.* 9:671–675. https://doi.org/10.1038/nmeth.2089

Schüller, C., Y.M. Mamnun, H. Wolfger, N. Rockwell, J. Thorner, and K. Kuchler. 2007. Membrane-active compounds activate the transcription factors Pdr1 and Pdr3 connecting pleiotropic drug resistance and membrane lipid homeostasis in *Saccharomyces cerevisiae*. *Mol. Biol. Cell.* 18:4932–4944. https://doi.org/10.1091/mbc.e07-06-0610

Setty, S.R., M.E. Shin, A. Yoshino, M.S. Marks, and C.G. Burd. 2003. Golgi recruitment of GRIP domain proteins by Arf-like GTPase 1 is regulated by Arf-like GTPase 3. *Curr. Biol.* 13:401–404. https://doi.org/10.1016/S0960-9822(03)00089-7

Setty, S.R., T.I. Strochlic, A.H. Tong, C. Boone, and C.G. Burd. 2004. Golgi targeting of ARF-like GTPase Arl3p requires its N^a-acetylation and the integral membrane protein Sys1p. *Nat. Cell Biol.* 6:414–419. https://doi.org/10.1038/ncb1121

Spang, A. 2015. The road not taken: less traveled roads from the TGN to the plasma membrane. *Membranes (Basel).* 5:84–98. https://doi.org/10.3390/membranes5010084

Thomas, L.L., and J.C. Fromme. 2020. Extensive GTPase crosstalk regulates Golgi trafficking and maturation. *Curr. Opin. Cell Biol.* 65:1–7. https://doi.org/10.1016/j.ceb.2020.01.014

Tie, H.C., D. Mahajan, B. Chen, L. Cheng, A.M. VanDongen, and L. Lu. 2016. A novel imaging method for quantitative Golgi localization reveals differential intra-Golgi trafficking of secretory cargoes. *Mol. Biol. Cell.* 27: 848–861. https://doi.org/10.1091/mbc.E15-09-0664

Tojima, T., Y. Suda, M. Ishii, K. Kurokawa, and A. Nakano. 2019. Spatiotemporal dissection of the *trans*-Golgi network in budding yeast. *J. Cell Sci.* 132:jcs231159. https://doi.org/10.1242/jcs.231159

Tsukada, M., E. Will, and D. Gallwitz. 1999. Structural and functional analysis of a novel coiled-coil protein involved in Ypt6 GTPase-regulated protein transport in yeast. *Mol. Biol. Cell.* 10:63–75. https://doi.org/10.1091/mbc.10.1.63

Tu, L., and D.K. Banfield. 2010. Localization of Golgi-resident glycosyltransferases. *Cell. Mol. Life Sci.* 67:29–41. https://doi.org/10.1007/s00018-009-0126-z

Valdivia, R.H., D. Baggott, J.S. Chuang, and R. Schekman. 2002. The yeast clathrin adaptor protein complex 1 is required for the efficient retention of a subset of late Golgi membrane proteins. *Dev. Cell.* 2:283–294. https://doi.org/10.1016/S1534-5807(02)00127-2

Voos, W., and T.H. Stevens. 1998. Retrieval of resident late-Golgi membrane proteins from the prevacuolar compartment of *Saccharomyces cerevisiae* is dependent on the function of Grd19p. *J. Cell Biol.* 140:577–590. https://doi.org/10.1083/jcb.140.3.577

Welch, L.G., and S. Munro. 2019. A tale of short tails, through thick and thin: investigating the sorting mechanisms of Golgi enzymes. *FEBS Lett.* 593: 2452–2465. https://doi.org/10.1002/1873-3468.13553

Wiederkehr, A., S. Avaro, C. Prescianotto-Baschong, R. Haguenauer-Tsapis, and H. Riezman. 2000. The F-box protein Rcy1p is involved in endocytic membrane traffic and recycling out of an early endosome in *Saccharomyces cerevisiae*. *J. Cell Biol.* 149:397–410. https://doi.org/10.1083/jcb.149.2.397

Wilcox, C.A., K. Redding, R. Wright, and R.S. Fuller. 1992. Mutation of a tyrosine localization signal in the cytosolic tail of yeast Kex2 protease disrupts Golgi retention and results in default transport to the vacuole. *Mol. Biol. Cell.* 3:1353–1371. https://doi.org/10.1091/mbc.3.12.1353

Wong, M., and S. Munro. 2014. The specificity of vesicle traffic to the Golgi is encoded in the golgin coiled-coil proteins. *Science.* 346:1256898. https://doi.org/10.1126/science.1256898

Zhdankina, O., N.L. Strand, J.M. Redmond, and A.L. Boman. 2001. Yeast GGA proteins interact with GTP-bound Arf and facilitate transport through the Golgi. *Yeast.* 18:1–18. https://doi.org/10.1002/1097-0061(200101)18:1<1::AID-YEA644>3.0.CO;2-5

Supplemental material

Table S1 lists the reagents and tools used in this study.

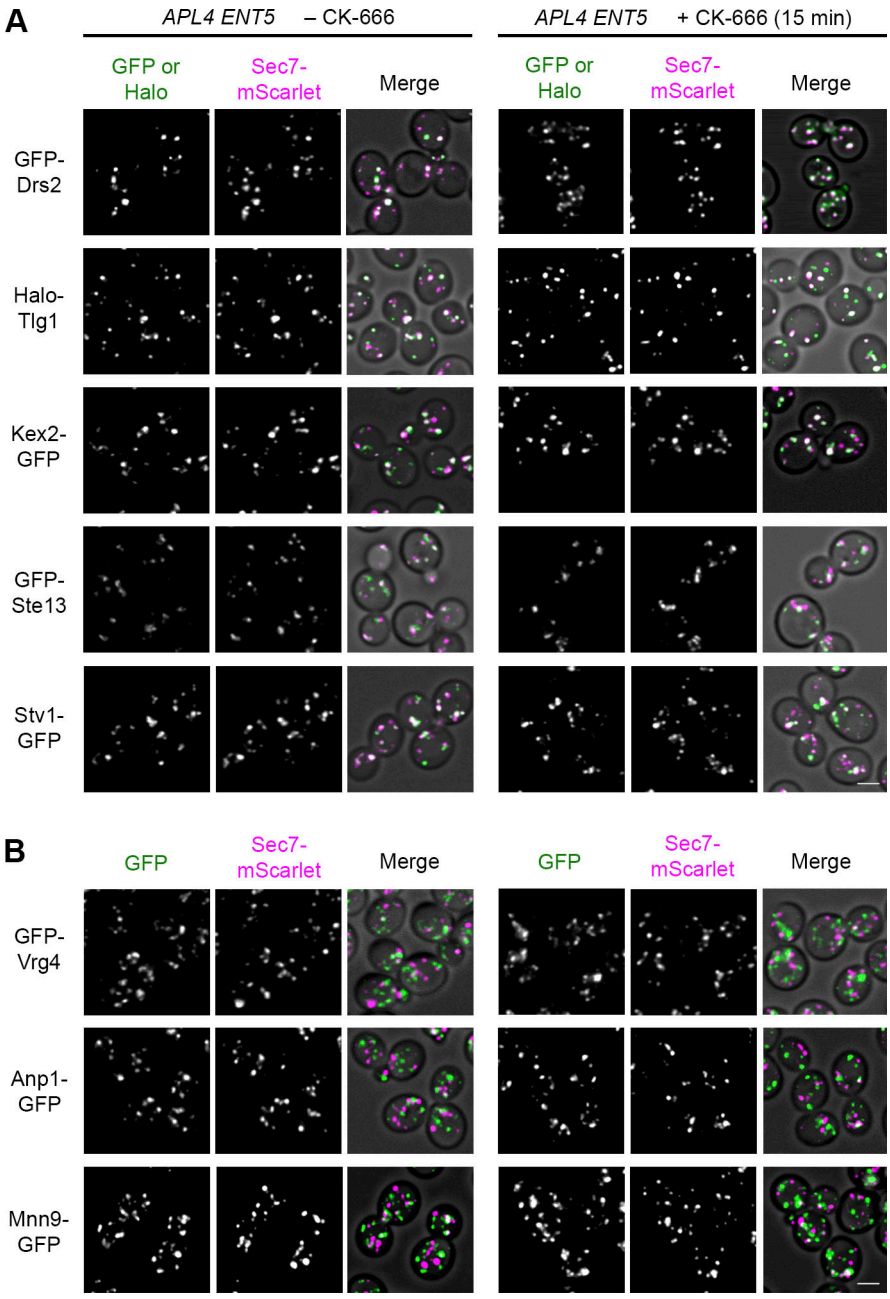

Figure S1. **CK-666 does not affect the localizations of transmembrane Golgi proteins in wild-type cells. (A)** Lack of a CK-666 effect on the localizations of transmembrane TGN proteins. The experiment was performed as in Fig. 3 D, except that *APL4 ENT5* cells were used and GFP-Ste13 and Stv1-GFP data are also shown. Scale bar, 2 µm. **(B)** Lack of a CK-666 effect on the localizations of transmembrane early Golgi proteins. The experiment was performed as in Fig. 3 D, except that *APL4 ENT5* cells were used and Anp1-GFP and Mnn9-GFP data are also shown. Scale bar, 2 µm.

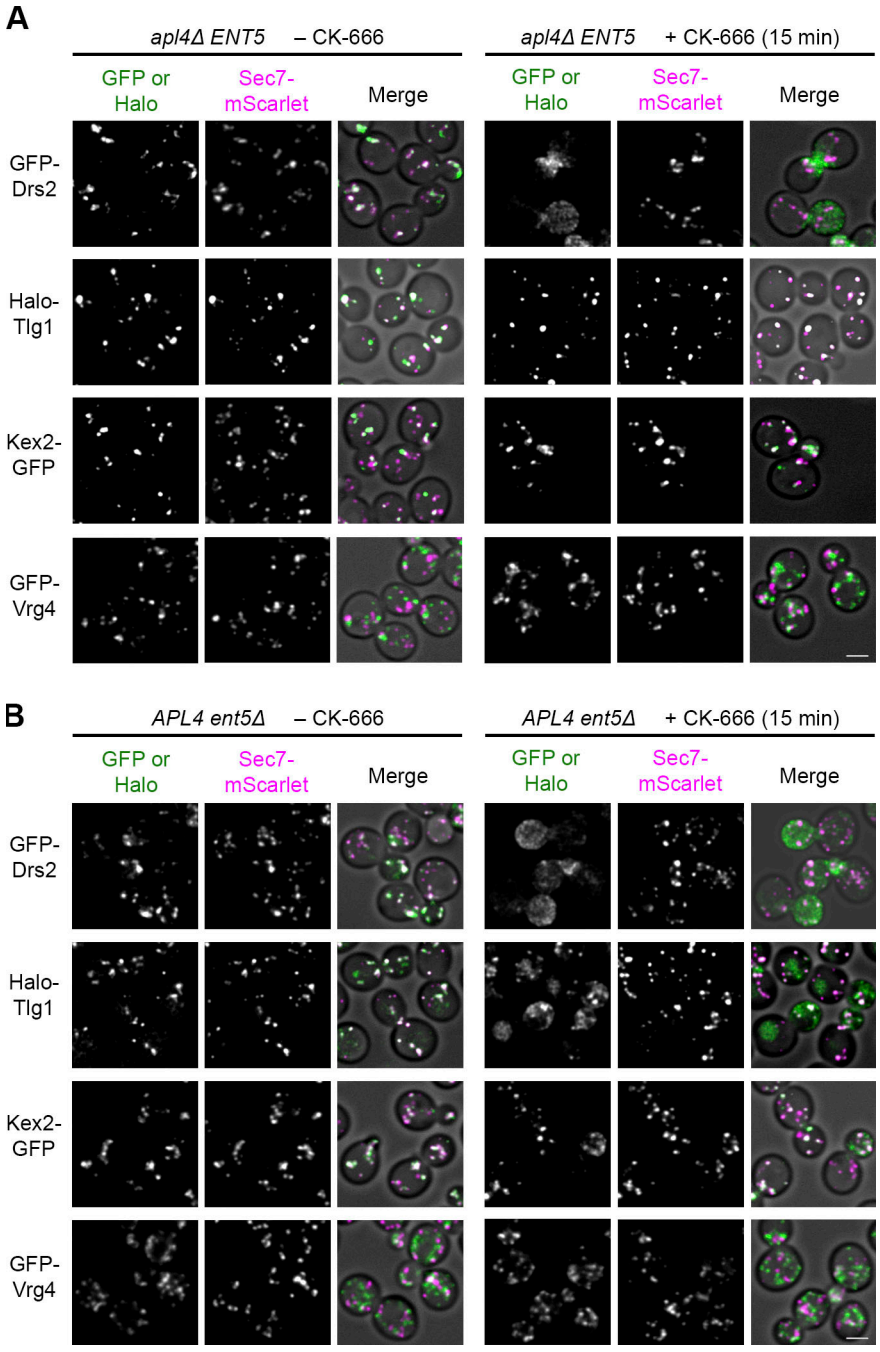

Figure S2. **CK-666 affects the localizations of some transmembrane TGN proteins in single mutant cells lacking either AP-1 or Ent5. (A)** Effect of CK-666 on the localizations of transmembrane TGN proteins in the absence of AP-1. The experiment was performed as in Fig. 3 D, except that *apl4Δ ENT5* cells were used. CK-666 caused mislocalization of Drs2 but not of Tlg1, Kex2, or Vrg4. Scale bar, 2 µm. **(B)** Effect of CK-666 on the localizations of transmembrane TGN proteins in the absence of Ent5. The experiment was performed as in Fig. 3 D, except that *APL4 ent5Δ* cells were used. CK-666 caused mislocalization of Drs2 and Tlg1 but not of Kex2 or Vrg4. Scale bar, 2 µm.

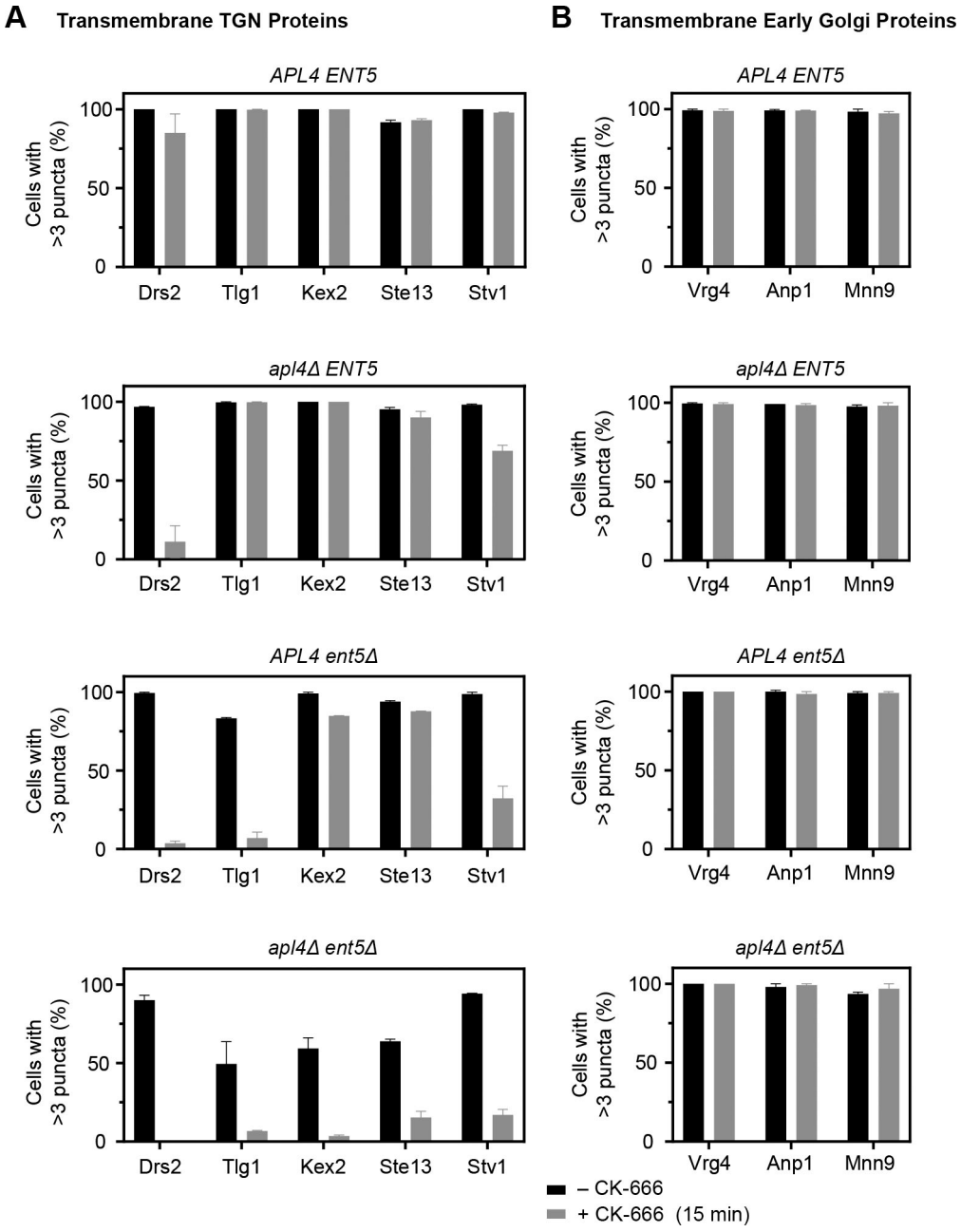

Figure S3. **CK-666 affects the localizations of transmembrane TGN proteins but not of transmembrane early Golgi proteins in double mutant cells lacking both AP-1 and Ent5. (A and B)** This figure extends Fig. 3 E, with the inclusion of additional marker proteins and of data from *apl4Δ ENT5* and *APL4 ent5Δ* cells. **(A)** Quantification of the CK-666 effects for five transmembrane TGN proteins in wild-type cells and in cells lacking either AP-1 or Ent5 or both. **(B)** Quantification of the CK-666 effects for three transmembrane early Golgi proteins in wild-type cells and in cells lacking either AP-1 or Ent5 or both. Error bars represent SEM.

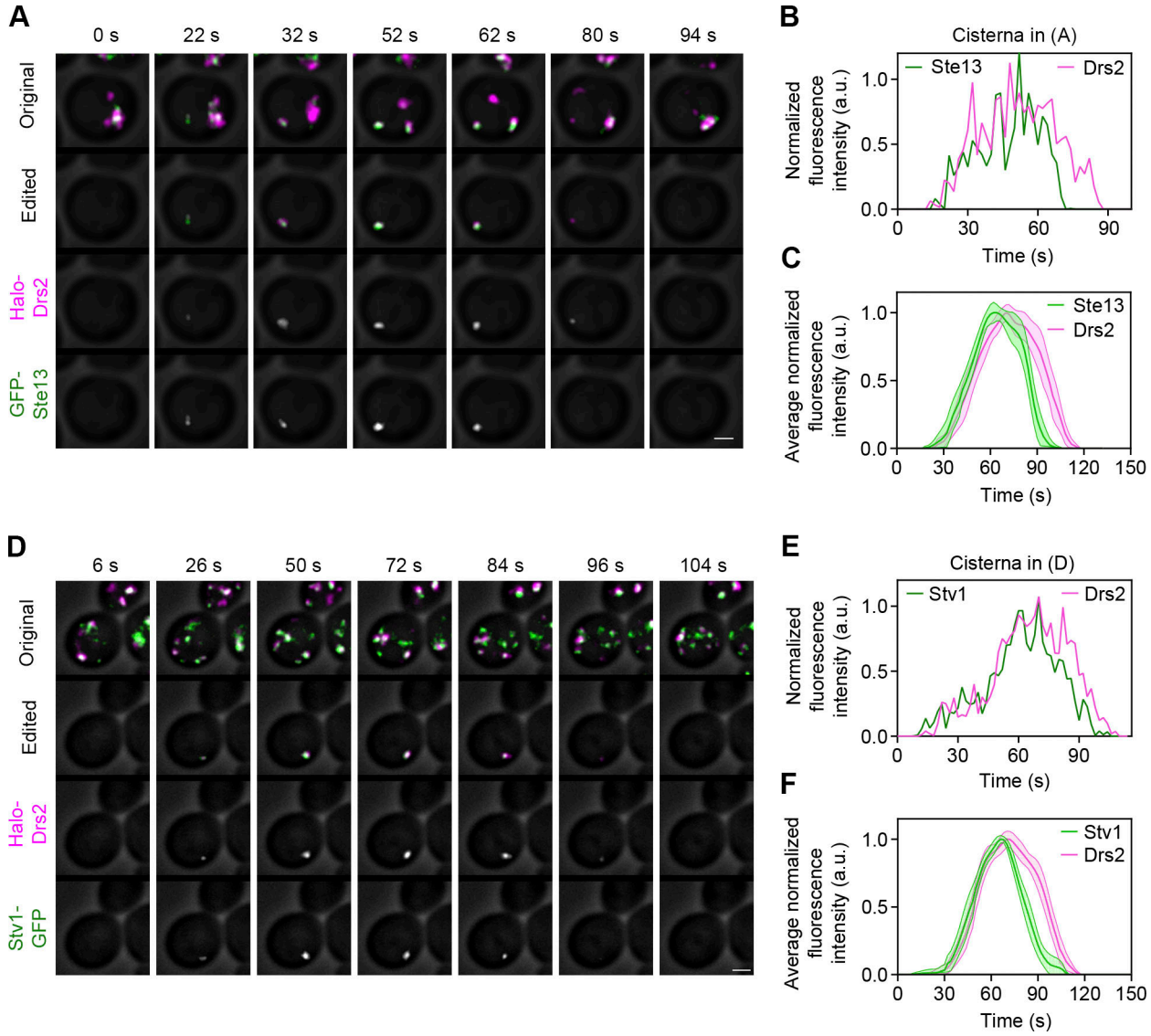

Figure S4. **Additional TGN proteins resemble Drs2 in their kinetic signatures. (A)** Maturation kinetics of Drs2 compared with Ste13. A strain expressing HaloTag-Drs2 and the dipeptidyl aminopeptidase GFP-Ste13 was grown to mid-log phase, labeled with JFX dye, and imaged by 4D confocal microscopy. Shown are average projected Z-stacks at the indicated time points from part 5 of Video 4. The upper row shows the complete projections, the second row shows edited projections that include only the cisterna being tracked, and the subsequent rows show the individual fluorescence channels from the edited projections. Scale bar, 2 µm. **(B)** Quantification of tagged Golgi proteins during a typical maturation event. Depicted are the normalized fluorescence intensities in arbitrary units for the cisterna tracked in A. **(C)** Smoothed and averaged traces showing the relative kinetic signatures of Drs2 and Ste13. Data were obtained for 10 representative cisternae. **(D)** Maturation kinetics of Drs2 compared with Stv1. The experiment was performed as in A, except that the strain expressed the proton-pumping ATPase subunit Stv1-GFP, and the images are from part 6 of Video 4. Scale bar, 2 µm. **(E)** Quantification of tagged Golgi proteins during a typical maturation event. Depicted are the normalized fluorescence intensities in arbitrary units for the cisterna tracked in D. **(F)** Smoothed and averaged traces showing the relative kinetic signatures of Drs2 and Stv1. Data were obtained for 15 representative cisternae.

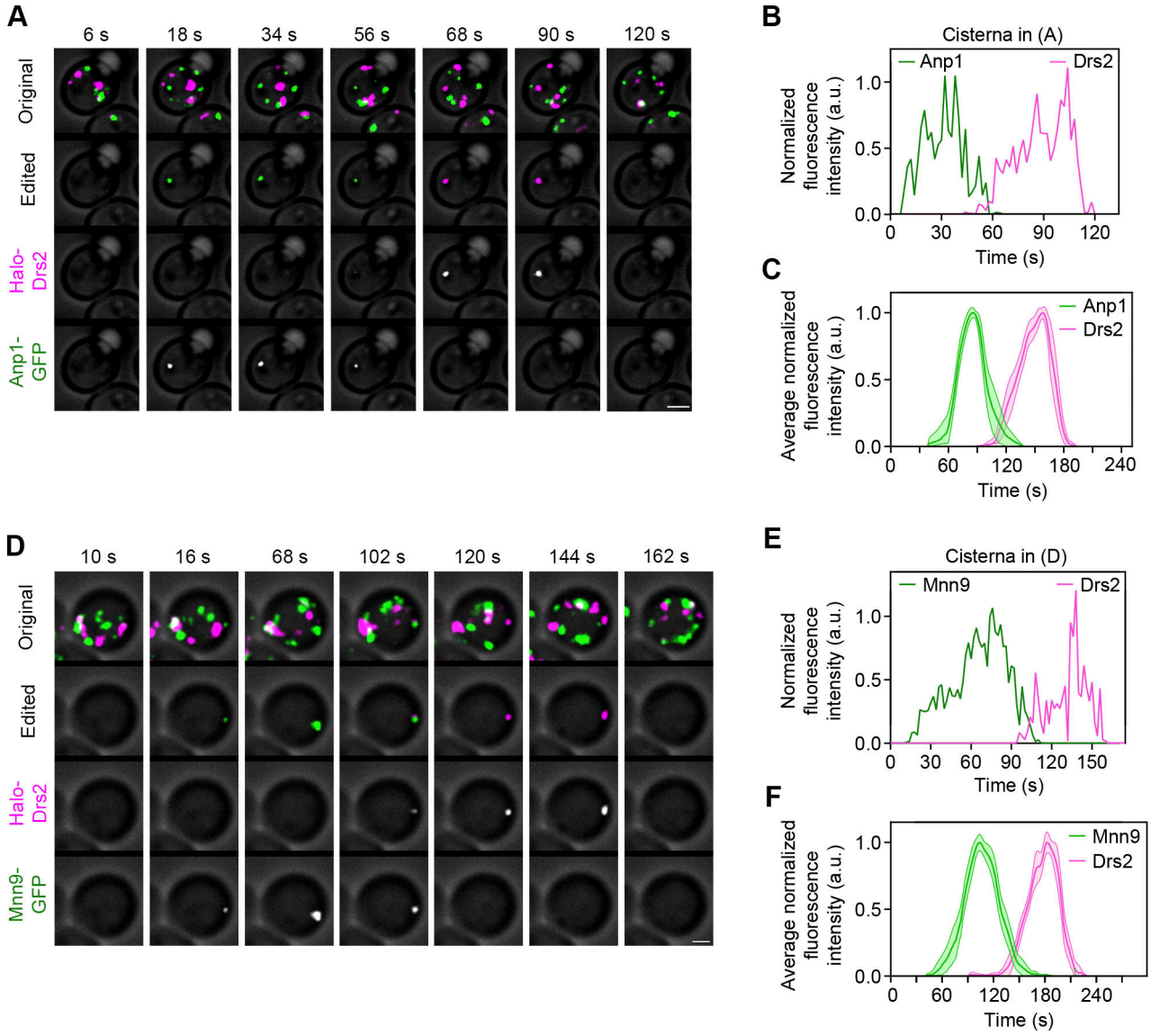

Figure S5. **Additional early Golgi proteins resemble Vrg4 in their kinetic signatures. (A)** Maturation kinetics of Drs2 compared with Anp1. A strain expressing HaloTag-Drs2 and the mannosyltransferase Anp1-GFP was grown to mid-log phase, labeled with JFX dye, and imaged by 4D confocal microscopy. Shown are average projected Z-stacks at the indicated time points from part 2 of Video 5. The upper row shows the complete projections, the second row shows edited projections that include only the cisterna being tracked, and the subsequent rows show the individual fluorescence channels from the edited projections. Scale bar, 2 µm. **(B)** Quantification of tagged Golgi proteins during a typical maturation event. Depicted are the normalized fluorescence intensities in arbitrary units for the cisterna tracked in A. **(C)** Smoothed and averaged traces showing the relative kinetic signatures of Drs2 and Anp1. Data were obtained for 10 representative cisternae. **(D)** Maturation kinetics of Drs2 compared with Mnn9. The experiment was performed as in A, except that the strain expressed the mannosyltransferase Mnn9-GFP, and the images are from part 3 of Video 5. Scale bar, 2 µm. **(E)** Quantification of tagged Golgi proteins during a typical maturation event. Depicted are the normalized fluorescence intensities in arbitrary units for the cisterna tracked in D. **(F)** Smoothed and averaged traces showing the relative kinetic signatures of Drs2 and Mnn9. Data were obtained for 13 representative cisternae.

Video 1. **AP-1 and Ent5 are present late in TGN maturation.** A strain expressing the TGN marker Sec7-mScarlet, the AP-1 subunit Apl2-GFP, and the clathrin adaptor Ent5-HaloTag was imaged as described in Fig. 1 A. Shown are average projected Z-stacks. Time is indicated in min:s format. The upper panel shows the complete projections, the second panel shows edited projections that include only a single representative cisterna, and the subsequent panels show the individual fluorescence channels from the edited projections. Scale bar, 2 µm. The frame rate is 15 fps (30× real time).

Video 2. **Golgi maturation is perturbed by CK-666 in a strain lacking AP-1 and Ent5.** Scale bars, 2 µm. Part 1: Normal Golgi dynamics in an untreated *apl4Δ ent5Δ* cell. A strain expressing the early Golgi marker GFP-Vrg4 and the TGN marker Sec7-mScarlet was imaged as described in Fig. 2 D. Shown are average projected Z-stacks. Time is indicated in min:s format. The upper panel shows the complete projections, the second panel shows edited projections that include only a single representative cisterna, and the lower two panels show the individual fluorescence channels from the edited projections. Parts 2 and 3: Abnormal Golgi dynamics in *apl4Δ ent5Δ* cells. The experiment was performed as in part 1, except that the cells were treated with CK-666 to block endocytosis as described in Fig. 2 F. In each case, the upper panel shows the complete projections and the lower panel shows edited projections that include only a single representative cisterna, which persistently contained either the early Golgi marker (part 2) or the TGN marker (part 3). The frame rate is 15 fps (30× real time).

Video 3. **Drs2 departure begins at about the same time as AP-1 arrival.** A strain expressing the TGN marker Sec7-mScarlet, the AP-1 subunit Apl2-GFP, and HaloTag-Drs2 was imaged as described in Fig. 3 A. Shown are average projected Z-stacks. Time is indicated in min:s format. The upper panel shows the complete projections, the second panel shows edited projections that include only two representative cisternae, and the subsequent panels show the individual fluorescence channels from the edited projections. Scale bar, 2 µm. The frame rate is 15 fps (30× real time).

Video 4. **Four transmembrane TGN proteins arrive and depart at about the same time as Drs2.** Each part of the video has the following format. Average projected Z-stacks are shown. Time is indicated in min:s format. The upper panel shows the complete projections, the second panel shows edited projections that include only a single representative cisterna, and the lower two panels show the individual fluorescence channels from the edited projections. Scale bars, 2 µm. Part 1: A strain expressing Kex2-GFP and Sec7-mScarlet was imaged as described in Fig. 4 A. Part 2: An *apl4Δ ent5Δ* strain expressing Kex2-GFP and Sec7-mScarlet was imaged as described in Fig. 4 D. Part 3: A strain expressing GFP-Drs2 and HaloTag-Tlg1 was imaged as described in Fig. 5 A. Part 4: A strain expressing HaloTag-Drs2 and Kex2-GFP was imaged as described in Fig. 5 D. Part 5: A strain expressing HaloTag-Drs2 and GFP-Ste13 was imaged as described in Fig. S4 A. Part 6: A strain expressing HaloTag-Drs2 and Stv1-GFP was imaged as described in Fig. S4 D. The frame rate is 15 fps (30× real time).

Video 5. **Three early Golgi proteins arrive and depart much earlier than Drs2.** Each part of the video has the following format. Average projected Z-stacks are shown. Time is indicated in min:s format. The upper panel shows the complete projections, the second panel shows edited projections that include only a single representative cisterna, and the lower two panels show the individual fluorescence channels from the edited projections. Scale bars, 2 µm. Part 1: A strain expressing HaloTag-Drs2 and GFP-Vrg4 was imaged as described in Fig. 5 G. Part 2: A strain expressing HaloTag-Drs2 and Anp1-GFP was imaged as described in Fig. S5 A. Part 3: A strain expressing HaloTag-Drs2 and Mnn9-GFP was imaged as described in Fig. S5 D. The frame rate is 15 fps (30× real time).

Video 6. **Proteins that travel from the TGN to PVE compartments depart earlier than Drs2.** Each part of the video has the following format. Average projected Z-stacks are shown. Time is indicated in min:s format. The upper panel shows the complete projections, the second panel shows edited projections that include only a single representative cisterna, and the lower two panels show the individual fluorescence channels from the edited projections. Scale bars, 2 µm. Part 1: A strain expressing HaloTag-Drs2 and Vps10-GFP was imaged as described in Fig. 6 A. Part 2: A strain expressing GFP-Drs2 and Nhx1-HaloTag was imaged as described in Fig. 6 D. The frame rate is 15 fps (30× real time).

Video 7. **The transmembrane Golgi protein Sys1 has an intermediate kinetic signature.** Each part of the video has the following format. Average projected Z-stacks are shown. Time is indicated in min:s format. The upper panel shows the complete projections, the second panel shows edited projections that include only a single representative cisterna, and the subsequent panels show the individual fluorescence channels from the edited projections. Scale bars, 2 µm. Part 1: A strain expressing Sec7-mScarlet, HaloTag-Drs2, and Sys1-GFP was imaged as described in Fig. 7 A. Part 2: An *apl4Δ ent5Δ* strain expressing Sec7-mScarlet and Sys1-GFP was imaged as described in Fig. 7 F. The frame rate is 15 fps (30× real time).

Video 8. **Two transmembrane Golgi proteins arrive and depart at about the same time as Sys1.** Each part of the video has the following format. Average projected Z-stacks are shown. Time is indicated in min:s format. The upper panel shows the complete projections, the second panel shows edited projections that include only a single representative cisterna, and the subsequent panels show the individual fluorescence channels from the edited projections. Scale bars, 2 µm. Part 1: A strain expressing HaloTag-Drs2 and Aur1-GFP was imaged as described in Fig. 8 C. Part 2: A strain expressing HaloTag-Drs2 and Rbd2-GFP was imaged as described in Fig. 8 F. The frame rate is 15 fps (30× real time).